Title

Emergence and Transmission of Arbovirus Evolutionary Intermediates with Epidemic Potential

Journal

Cell Host & Microbe, 15(6)

ISSN

1931-3128

Authors

Stapleford, Kenneth A

Coffey, Lark L

Lay, Sreyrath

et al.

Publication Date

2014-06-01

DOI

10.1016/j.chom.2014.05.008

Emergence and Transmission of Arbovirus Evolutionary Intermediates with Epidemic Potential

Kenneth A. Stapleford,[1] Lark L. Coffey,[2] Sreyrath Lay,[3] Antonio V. Bordería,[1] Veasna Duong,[3] Ofer Isakov,[4] Kathryn Rozen-Gagnon,[1] Camilo Arias-Goeta,[5] Hervé Blanc,[1] Stéphanie Beaucourt,[1] Türkan Haliloğlu,[6] Christine Schmitt,[7] Isabelle Bonne,[7] Nir Ben-Tal,[8] Noam Shomron,[4] Anna-Bella Failloux,[5] Philippe Buchy,[3] and Marco Vignuzzi[1,*]

[1]Viral Populations and Pathogenesis Unit, Institut Pasteur, Centre National de la Recherche Scientifique UMR 3569, 28 rue du Dr Roux, 75724 Paris Cedex 15, France
[2]Center for Vectorborne Diseases, Department of Pathology, Microbiology and Immunology, School of Veterinary Medicine, University of California, Davis, One Shields Avenue, 5327 VM3A, Davis, CA 95616, USA
[3]Virology Unit, Institut Pasteur in Cambodia 5, Monivong Boulevard, PO Box 983, Phnom Penh, Cambodia
[4]Sackler Faculty of Medicine, Tel Aviv University, Tel Aviv 69978, Israel
[5]Arboviruses and Insect Vectors Lab, Institut Pasteur, 25 rue du Dr Roux, 75724 Paris Cedex 15, France
[6]Department of Chemical Engineering and Polymer Research Center, Boğaziçi University, Bebek 34342, Istanbul, Turkey
[7]Ultrastructural Microscopy Platform, Institut Pasteur, 28 rue du Dr Roux, 75724 Paris Cedex 15, France
[8]Department of Biochemistry and Molecular Biology, George S. Wise Faculty of Life Sciences, Tel Aviv University, Tel Aviv 69978, Israel
*Correspondence: marco.vignuzzi@pasteur.fr
http://dx.doi.org/10.1016/j.chom.2014.05.008

SUMMARY

The high replication and mutation rates of RNA viruses can result in the emergence of new epidemic variants. Thus, the ability to follow host-specific evolutionary trajectories of viruses is essential to predict and prevent epidemics. By studying the spatial and temporal evolution of chikungunya virus during natural transmission between mosquitoes and mammals, we have identified viral evolutionary intermediates prior to emergence. Analysis of virus populations at anatomical barriers revealed that the mosquito midgut and salivary gland pose population bottlenecks. By focusing on virus subpopulations in the saliva of multiple mosquito strains, we recapitulated the emergence of a recent epidemic strain of chikungunya and identified E1 glycoprotein mutations with potential to emerge in the future. These mutations confer fitness advantages in mosquito and mammalian hosts by altering virion stability and fusogenic activity. Thus, virus evolutionary trajectories can be predicted and studied in the short term before new variants displace currently circulating strains.

INTRODUCTION

A hallmark of RNA viruses is that rapid replication with high mutation rates can result in the emergence of new epidemic variants (Domingo, 2010). Unfortunately, such variants are usually identified retrospective to epidemics (Davis et al., 2005; Schuffenecker et al., 2006) because wide-scale monitoring of circulating strains is time and labor intensive, and predicting long-term evolution is complicated by ecological factors (Holmes, 2013; Weaver and Barrett, 2004). Recent studies in the adaptation of H5N1 influenza virus to droplet transmission in ferrets exemplifies how evolutionary experiments can shed light on the adaptive pathways available to RNA viruses to increase fitness in a new host (Herfst et al., 2012; Imai et al., 2012). These studies underscore the need to better target surveillance of current strains and predict their evolution, at least in the short term, with more confidence (Holmes, 2013). Since surveillance currently relies on consensus sequencing, adaptive mutations are masked by wild-type sequence and only identified once they dominate the virus population, a process that can take months or years. Depending on the virus under study, the likelihood of identifying emerging variants in a circulating strain can be further hindered by the nature of the isolate: (a) amplification and passage of primary isolates in cell culture can alter the composition of mutants within the population; (b) pooling of samples can dilute the abundance of an emerging variant; and (c) the anatomical origin of the sample may not represent the virus population most likely to be transmitted.

Retrospective studies attempting to experimentally recapitulate and mechanistically explain emergence events from previous epidemics have had some success. For example, in 2005/2006 an epidemic of chikungunya virus that normally circulates in *Aedes aegypti* mosquitoes occurred in the Indian Ocean islands when an alanine-to-valine mutation at residue 226 of the E1 glycoprotein (A226V) promoted enhanced infectivity of another mosquito vector, *Aedes albopictus* (Schuffenecker et al., 2006; Tsetsarkin et al., 2007; Vazeille et al., 2007). Subsequent studies uncovering epistatic interactions of A226V with previously acquired E2 glycoprotein mutations revealed a stepwise evolutionary trajectory that partly explains the delay in its emergence (Tsetsarkin et al., 2011). An ecological factor likely impacting this emergence was the abundance of *Ae. albopictus*

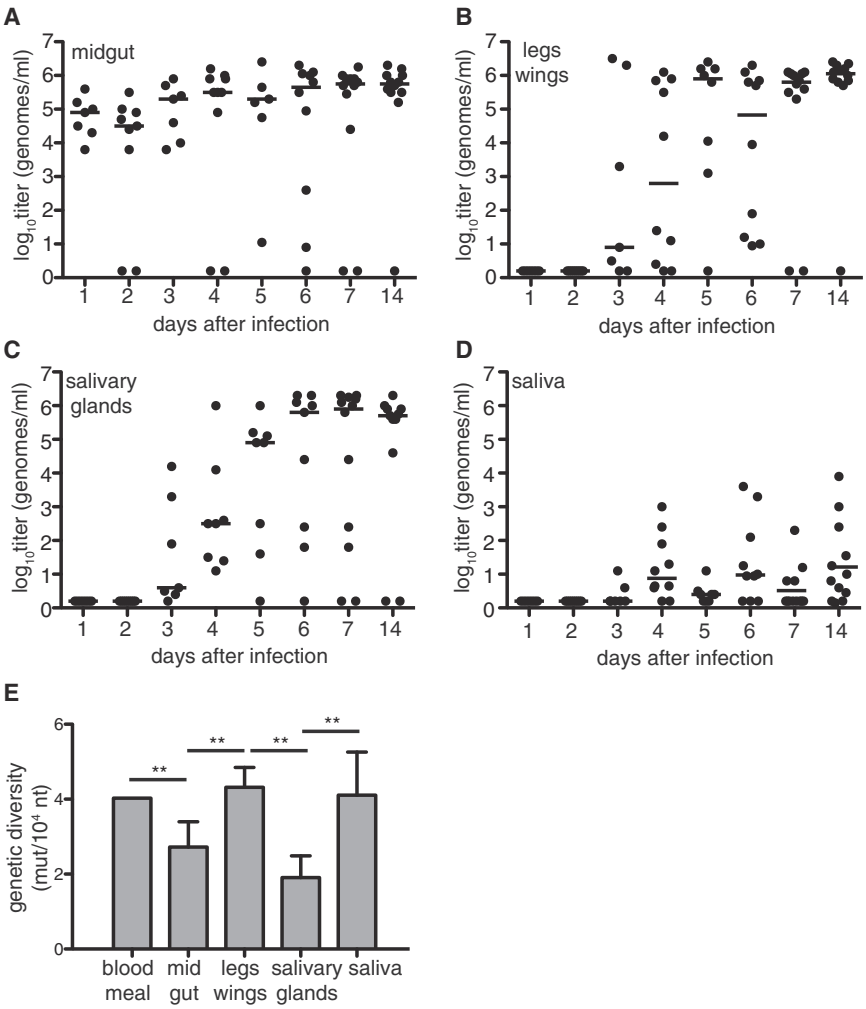

Figure 1. Infection Kinetics and Population Dynamics of Chikungunya Virus in Mosquitoes

(A–D) At indicated days after feeding on blood meals containing 10^6 pfu/ml of chikungunya virus, virus titers were assayed by qRT-PCR in (A) midguts, (B) legs/wings, (C) salivary glands, and (D) saliva from *Aedes aegypti* mosquitoes. Titers for individual mosquitoes (scatter plot) and median (bar) are shown.

(E) The mean genetic diversity present in blood meals, midguts, legs/wings, salivary glands, and saliva from individual mosquitoes 7 days after infection, represented as the average number of mutations per 10^4 nt sequenced. A general trend of reduction in genetic diversity at known anatomical barriers confirms the presence of population bottlenecks (midgut, salivary glands). Between 70 and 96 clones and an average of 82,000 nt were sequenced per sample; n = 6 mosquitoes; **p < 0.01 by X^2 test.

and near lack of *Ae. aegypti* in the Indian Ocean islands compared to endemic regions (Tsetsarkin et al., 2007). Taken together, these conditions created an optimal environment for the emergence of A226V, a problematic event given the world-wide distribution of *Ae. albopictus*. However, although the adaptive mutation required a single nucleotide substitution, the emergence of this variant in nature required years to occur, and as a result the aforementioned studies were performed after the fact. Here, we show that emergence events that require years to identify in nature can be more readily identified and predicted by monitoring transmission site-specific virus subpopulations during experimental infection and transmission in vivo.

RESULTS

Chikungunya Virus Infection Dynamics and Population Bottlenecks

Given that higher fitness variants remain undetected until they displace wild-type after repeated infection and spread across hosts, we hypothesized that studying the spatial and temporal evolution of these viruses in vivo could more quickly identify evolutionary intermediates prior to emergence. Since mosquitoes are persistent carriers of arboviruses, we first optimized experimental conditions by infecting *Ae. aegypti* mosquitoes with chikungunya virus and monitoring replication in midguts (first site of replication), legs and wings (disseminating population), salivary glands (final site of replication), and saliva (transmitted population) (Figures 1A–1D). The initial infection of midguts was followed by increasing titers of circulating and transmitted virus that peaked 7 days after infection. To study whether virus populations differed upstream and downstream of known anatomical barriers, we determined the relative viral genetic diversity in compartment-specific subpopulations at peak titers. Fluctuations in the global genetic diversity in each compartment are in accordance with two population bottlenecks expected to coincide with anatomical barriers in midguts and salivary glands (Figure 1E) that were previously confirmed for West Nile and Venezuelan equine encephalitis viruses (Ciota et al., 2012; Forrester et al., 2012).

Emergence of the Chikungunya Virus E1 A226V Indian Ocean Epidemic Strain in the Saliva of Mosquitoes Infected with the Pre-epidemic Strain

To study the predictive power to identify evolutionary intermediates with this approach, we focused on the viral subpopulations transmitted in the saliva of individual mosquitoes after the peak of infection. We asked whether we could recapitulate the emergence of the E1 A226V amino acid change responsible for the Indian Ocean epidemic (Schuffenecker et al., 2006; Tsetsarkin et al., 2007; Vazeille et al., 2007). We infected both *Ae. aegypti* and *Ae. albopictus* mosquitoes with the pre-epidemic strain (alanine at residue 226) and deep sequenced individual mosquito saliva samples 10 days after infection (Table 1). All ten *Ae. aegypti* mosquitoes presented only the original strain with no detectable changes at residue 226 (limit of detection < 0.01%). In contrast,

Table 1. Identification of E1 Glycoprotein Variants A226V and V80I:A129V in Transmission Compartments of Mosquitoes of Different Geographical Origin

Nature of Sample	Mosquito No.[a]	Mutation (%)	
		A226V (%)	
A226 pre-epidemic stock[b]	n/a	<0.01	
Ae. aegypti saliva Nakhon Chum, Thailand	1–10	0.016–0.04	
Ae. albopictus saliva[c] Phu Hoa, Vietnam	1	11.65	
	2	9.12	
	3	99.91	
	4	0.03	
Ae. albopictus matched bodies[c] Phu Hoa, Vietnam	1	0.07	
	2	0.09	
	3	0.08	
	4	<0.01	
		V80I (%)	A129V (%)
A226V postepidemic stock[d]	n/a	0.06	0.01
Ae. aegypti saliva[e] Rockefeller Colony	1	10.55	68.21
	2	9.01	56.39
	3	10.00	49.82
	4	21.98	55.21
	5–8	<0.01	<0.01
Ae. aegypti matched salivary gland[e] Rockefeller Colony	1	0.015	0.020
	2	<0.01	0.032
	3	<0.01	0.021
	4	0.011	0.017
	5	<0.01	<0.01
	6	<0.01	<0.01
	7	<0.01	<0.01
	8	<0.01	<0.01
Ae. aegypti saliva Bénoué, Cameroon	1	10.89	70.02
	2	0.06	0.07
	3	0.11	0.11
	4	0.05	0.11
	5	5.38	5.81
	6	0.06	0.11
	n/a	21.06	22.27
	7–8	<0.01	<0.01
Ae. aegypti saliva Paea, Tahiti	1	69.03	69.86
	2	16.03	16.53
	3	43.36	44.11
	4–7	<0.01	<0.01
Ae. albopictus saliva Bertoua, Cameroon	1	98.75	98.74
	2	34.28	10.52
	3	0.21	0.23
	4	46.01	47.09
	5	99.69	99.67
	6	0.18	0.28
	7	0.05	0.11
	8–10	<0.01	<0.01
2012 Cambodian patient stock[f]	n/a	<0.01	<0.01
Ae. aegypti saliva Kampong Cham, Cambodia	1	0.14	0.22
	2	51.92	52.70
	3	0.10	0.12
	4	58.87	59.96
	5	1.70	1.74
	6	57.07	58.56

[a]When either mutation of interest could be detected above background, the individual values are shown; the grouped mosquitoes only presented the original strain with no detectable mutations at these sites; the limit of detection < 0.01% is then given.
[b]The pre-2005/2006 epidemic stock, presenting an alanine at position 226, used to infect mosquitoes.
[c]Deep sequencing of matched saliva and body samples from individual mosquitoes.
[d]The parental A226V virus stock, corresponding to the 2005/2006 Indian Ocean epidemic strain, used to infect mosquitoes in this study.
[e]Deep sequencing of matched saliva and salivary gland samples from individual mosquitoes. See also Table S1.
[f]The 2012 isolate obtained from a Cambodian patient used to infect mosquitoes.

we detected the A226V mutation in three of four *Ae. albopictus* mosquito saliva samples (at 9%, 11%, and 99% total virus population). A226V was the only mutation emerging at a high frequency in these transmission samples, confirming that our approach could have predicted the emergence of the 2006 epidemic strain in as little as 10 days of infection in vivo. Importantly, the abundance of these mutations in saliva was considerably higher than in the corresponding mosquito bodies (Table 1), thus highlighting the biological relevance of specifically monitoring transmissible subpopulations.

Emergence of Chikungunya Virus E1 Variants in the Saliva of Mosquitoes Carrying the Currently Circulating Indian Ocean Epidemic A226V Strain

Given the success in rapidly identifying the A226V adaptation that required years to emerge in nature, we asked whether infecting mosquitoes with the post-2005/2006 epidemic strain could identify future emergence events. *Ae. aegypti* and *albopictus* mosquitoes (established lab colonies and recently captured from African and Asian locations) were infected for 10 days with the A226V strain, and saliva samples were deep sequenced in the E1 glycoprotein gene. In all four experiments, two mutations (V80I and A129V) were the only mutations to amplify to significantly high frequency in the saliva of multiple mosquitoes (Tables 1 and S1). Since saliva is a cell-free environment, replication of these variants would have expectedly occurred in salivary glands. Indeed, mosquitoes with high frequencies of V80I and A129V in saliva presented these mutations at low, yet significant, frequency in salivary glands, whereas no mutations could be detected in the glands of saliva-negative mosquitoes (Table 1). Furthermore, molecular cloning and Sanger sequencing of 70–96 genomes per population confirmed that these mutations,

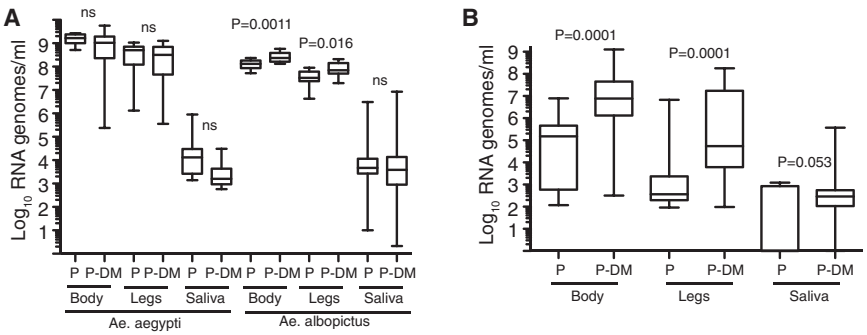

Figure 2. The P-DM Strain Presents an Increased Replication Advantage in Mosquito Hosts

(A) High-dose infection (10^6 pfu/ml) of *Ae. aegypti* and *Ae. albopictus* mosquitoes with the parental A226V strain (P) or with the additional two mutations V80I:A129V (P-DM). Virus titers were determined 7 days after infection in bodies, legs/wings, and saliva by qRT-PCR. Significant p values are indicated. ns, no significant difference observed between P and P-DM ($p > 0.5$); n = 30; two-tailed unpaired Student's t test; box plots show median value and minimum and maximum values.

(B) Low-dose infection (10^3 pfu/ml) of *Ae. albopictus* mosquitoes. Significant p values are indicated. ns, no significant difference ($p > 0.5$); n = 20; two-tailed unpaired Student's t test; box plots show median value and minimum and maximum values.

when present at equal frequencies, were always linked on the same genome (data not shown).

Emergence of V80I:A129V in Cambodian Mosquitoes Infected with a Currently Circulating A226V Isolate from a Cambodian Patient

Since the infectious clone used in the lab was derived from a 2006 A226V isolate obtained from a patient in La Réunion Island, we investigated whether similar emergence events can occur in more recent circulating strains. We infected Cambodian *Ae. aegypti* mosquitoes that were recently caught in the wild (F2 generation) with a recent 2012 isolate from a Cambodian patient. After 10 days of infection, the V80I:A129V mutations were once more the only mutations to be identified in the saliva of all six mosquitoes (Table 1), providing further evidence that these mutations are evolutionary intermediates of currently circulating strains.

Chikungunya Virus V80I:A129V Mutations Confer Replication Advantages to the A226V Strain in Mosquitoes

We explored whether the V80I and A129V mutations incur an advantage in vivo or whether they represent "transmission dead ends" with no biologically relevant advantage. Starting from the parental A226V infectious clone (P), we engineered the double-mutation V80I:A129V (P-DM) and compared the strains in terms of infection (bodies), dissemination (legs and wings), and transmission (saliva) in both mosquito hosts. At high-infection doses (10^6 plaque-forming units [pfu]/ml), P-DM strain presented the same titers as the parental strain in *Ae. aegypti* and significantly higher infection ($p = 0.0011$) and dissemination ($p = 0.016$) titers in *Ae. albopictus* (Figure 2A). Since mosquitoes in nature are exposed to a wide range of viremic titers in mammalian hosts, we repeated the *Ae. albopictus* infection using lower doses (10^3 pfu/ml). At a low dose, the P-DM strain presented more significant infection ($p = 0.0001$), dissemination ($p = 0.0001$), and transmission ($p = 0.053$) titers (Figure 2B). Since the E1 mutations arose in both mosquito species (Table 1), yet a benefit was only observed in *Ae. albopictus*, we sequenced a high and low titer saliva sample from the A226V-infected *Ae. aegypti* mosquitoes characterized in Figure 2A. The high titer "parental" sample had in fact already evolved into the P-DM genotype by the time the sample was taken, indicating that the relatively equal fitness observed for P-DM in this species may be underestimated in our experiment.

P-DM Strain Leads to Increased Viral Loads and Pathogenesis in a Mammalian Infection Model

To examine the impact of the V80I:A129V mutations in the mammalian host, we infected a small rodent infection model (8-day-old mice) (Couderc et al., 2008) with lethal doses (10^6 pfu) of parental virus compared to the P-DM strain and monitored survival (Figure 3A). Since chikungunya virus is not generally fatal in humans (Manimunda et al., 2011; Renault et al., 2008), this model is not representative of CHIKV pathogenesis; rather, virulence and tropism in these mice is a close surrogate for replicative capacity in mammals (Couderc et al., 2008; Ozden et al., 2007; Ziegler et al., 2008). Infection of newborn mice resulted in 40% mortality by 14 days of infection with parental virus and 100% mortality by 6 days of infection with P-DM. As expected, adult mice showed no signs of virulence with either strain (Figure 3A). To confirm this presumed increase in replicative capacity, we administered a sublethal dose (10^2 pfu) to 8-day-old mice and titrated virus in different organs. Virus titers were significantly higher (up to 100-fold) for the new strain in both blood and muscle (Figure 3B).

The V80I:A129V Mutations Alter Fusion Activity and Particle Stability In Vitro

To address the molecular mechanisms underlying the fitness advantages observed in vivo, we compared tissue culture phenotypes of the P-DM strain, as well as each individual mutation (P-V80I and P-A129V), to the parental A226V virus. We did not observe significant advantages or defects for most traits relating to the virus life cycle under the standard cell culture conditions (receptor binding, entry via endocytic pathways, RNA synthesis, and E1 glycoprotein expression; Figure S1). Electron microscopy of infected mosquito and human cells revealed no differences in cell and virus morphology or budding (Figure S2). We thus compared the production of infectious virus in a larger panel of cell lines. The yield of the P-DM strain was similar to parental virus in most cell lines assayed and significantly higher in one murine and two human lines (Figure 4A), in accordance with the increased replication observed in the mouse model (Figure 3B). Based on the crystal structure of the E1 glycoprotein,

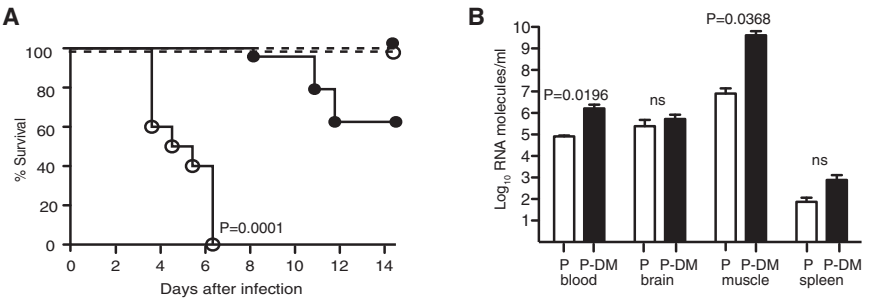

Figure 3. The P-DM Strain Presents Increased Viral Loads and Pathogenesis in a Mammalian Host

(A) Survival of 8-day-old (solid lines) or 3-week-old (dashed lines) C57BL/6 mice inoculated with 10^6 pfu of the parental strain (solid circle) or P-DM (open circle). $p < 0.0001$; n = 12; log-rank Mantel-Cox test.

(B) Tissue-specific virus titers 7 days after sublethal infection (200 pfu) of mice infected with parental strain (P) or P-DM. p values are shown; ns, no significant difference observed between P and P-DM ($p > 0.5$); n = 4–6 mice per day; two-tailed unpaired t test.

we performed normal mode analysis to identify potential effects of residues 80 and 129 on function. Slow and fast mode analysis suggested an implication in conformational changes during fusion and/or in structural stability of the virion (Figures 4B and S3). To address the fusion activity of each virus in detail, we performed fusion from without assays using a GFP-expressing parental (P-GFP), individual (P-V80I-GFP and P-A129V-GFP), and double mutation (P-DM-GFP) containing viruses on baby hamster kidney (BHK) and mouse embryonic fibroblast (MEF) cells using a range of pH from 5.0 to 7.4. Fusion activity was similar for all viruses over this range, but P-DM-GFP virus had significantly higher fusion at the most relevant pH range (pH 5.4–5.8) (Figures 4C and 4D). The A129V single mutation also showed trends in increased fusion that were significant in one instance (Figure 4C). In addition, we treated GFP-expressing viral stocks with the same panel of pH buffers to "pre-trigger" a conformational change in the E1 glycoprotein prior to infection. As in the cellular fusion assay, fusion was triggered at significantly higher levels (thus, lower residual infectivity following pretreatment) for P-DM-GFP at several pH values, and both single mutations more readily fused at pH 5.8 compared to the parental strain (Figure 4E). Finally, fusion activity was examined in the presence of four different fusion-blocking antibodies. In three of four cases, the P-DM strain retained a more significant level of fusion activity (Figure 4F). To address particle stability, we incubated viruses in cell-free suspension at 28°C (mosquito temperature) and at 37°C (mammalian temperature) (Figure 4G). The single mutants P-V80I, P-A129V, and the P-DM strain presented increased stability at both temperatures, notably retaining up to 95% of their specific infectivity after 48 hr at mosquito temperature compared to 10% of parental virus.

Emergence and Dominance of the P-DM Strain during Natural Transmission

Since the V80I:A129V mutations were found to have significant fitness advantages in vitro and in vivo in both mosquito and mammalian hosts, we addressed the evolution of the parental A226V strain in the most natural experimental setting possible. To do so, we established an infection and transmission model (Figure 5A) where individual African *Aedes aegypti* mosquitoes were infected with the parental strain and fed on individual mice, which in turn were fed to a second batch of mosquitoes. At each transmission step, individual bodies and saliva of mosquitoes and blood of mice were deep sequenced. Following the first transmission of 18 infected mosquitoes to mice (Figure 5B), six mice failed to present virus in blood and could not transmit to the second batch of mosquitoes, and one mouse succumbed to infection before this second transmission step. For the remaining 11 infected mice, each further transmitted virus to at least two naive mosquitoes (every engorged mosquito that fed on mice became positive for CHIKV by 10 days postfeeding). Deep sequencing of the saliva populations of eight of the initially infected mosquitoes (series #1–8) revealed the emergence of the P-DM strain at frequencies ranging from 0.25% to 99.68% (Figure 5B). When present in saliva, this strain was transmitted to mice, where its frequency fluctuated without an apparent positive or negative trend yet remained the most abundant minority genotype in the blood (Figure 5B). Of the 24 naive mosquitoes that fed on these mice during the second transmission step (series #1–8), 18 presented P-DM at very high frequency in their bodies, which was further amplified in saliva to displace the parental A226V strain. For mice that did not present V80I and A129V in the blood (#10–12), only the original A226V strain was transmitted to naive mosquitoes, yet four of these mosquitoes also developed the P-DM variant in saliva de novo, similar to the initial infection of the first batch of mosquitoes. We analyzed the dynamics of these variants in different compartments (Figure 5C) and identified two potential events of positive selection (Figure S4). One was revealed by a positive correlation between the presence of P-DM in the blood of mice and its amplification in the bodies of mosquitoes feeding upon them ($p = 0.037$), while the other was revealed by a correlation between the P-DM frequencies in mosquito bodies compared to saliva in both mosquito batches ($p = 0.012$ and 0.004). Similar results were obtained in a second experiment using Asian *Ae. aegypti* mosquitoes (Figure S5). In summary, the data indicate that the P-DM strain is a genotype capable of emerging and displacing the parental A226V epidemic strain during natural transmission from mosquitoes to mammals.

DISCUSSION

In this study, we developed an experimental approach to monitor the selection and emergence of a strain of chikungunya that proved to be epidemic (A226V) as well as the continued evolution of this strain to contain two E1 mutations (V80I and A129V). Importantly, these mutations were the only ones to arise above the 0.01%–0.2% frequency range that encompassed the remainder of minority variants in the viral populations in multiple mosquitoes of both African and Asian origin (Table S1).

Interestingly, although replication of these variants occurred in the mosquito body (e.g., midgut, salivary gland), they were enriched to high frequencies in the saliva compartment. We attribute the success of this approach to several improvements over the more conventional protocols in studying, and trying to predict, virus evolution and emergence. First, mosquitoes are rarely sampled beyond the day that peak titers are reached (for chikungunya, 7 days), which may not be sufficient time for adaptive mutations to be generated and amplified. Indeed, the mutations described here could not be detected during the first 5 days of infection (data not shown). Moreover, pooling of samples would have diluted the high frequency variants present in a few mosquitoes to the limit of detection. Even within individual mosquitoes, the highest-frequency variants present in saliva would have been lost in the background of the body and salivary gland populations, where titers can be over three orders of magnitude higher. Finally, without deep sequencing, emerging mutations would not have been detected in enough individuals to differentiate them from stochastic mutations occurring within each mosquito. Our results have significant implications for current surveillance strategies during and between epidemics. The fact that the A226V mutation was the only one to occur at high frequency in multiple *Ae. albopictus* mosquitoes could have alerted us to a potential emergence event well before it took hold in nature. That A226V arose to high frequencies in mosquitoes in only 10 days, while it took several years to emerge in nature, suggests that ecological factors play the final decisive role on which variants emerge, following selection within the host.

The natural transmission studies presented here suggest that selection of the P-DM strain occurs in two different stages of the infection cycle (Figure S4). The high frequencies of these mutations in saliva compared to salivary glands suggest a selective step after virus replication and egress into a cell-free environment. As suggested by molecular modeling and confirmed by in vitro stability studies, the P-DM variant retains infectivity for periods significantly longer than those of parental A226V in cell-free conditions. Thus, although both strains have similar replication kinetics and yields, the superior survival of V80I:A129V-containing virion outside of host cells (particularly at mosquito temperatures) could account for their temporal increase in abundance in saliva samples. If this increased stability and specific infectivity confers a similar advantage during extracellular stages in the host (e.g., circulating in the hemocoel of mosquitoes or bloodstream of mammals), this effect may partially account for the increased titers of virus observed in mosquito and mouse tissues. However, since molecular modeling, fusion assays, and infections in the presence of fusion-blocking antibodies also showed that P-DM is better able to enter cells under more stringent conditions, increased fusogenic activity may play the more significant role during selection in mosquito bodies, before egress into saliva. Increased fusion may also account for the higher fitness of P-DM observed in some human and murine cell lines. Positive selection for mutations V80I and A129V is thus a combination of improved stability and fusogenic activity, as evidenced by the predominance and further implication of this strain in bodies and saliva of mosquitoes feeding on mice that have P-DM in their blood. Normal mode analysis suggests that these residues may be part of an epistatic network that includes position 226, which may explain why these mutations were observed in every experiment using A226V, but not in the mosquitoes infected with the pre-epidemic A226 strain. Further work is required to determine whether the V80I and A129V mutations would confer fitness advantages to strains carrying alanine at position 226.

Whether these mutations will emerge in nature will depend on many ecological factors, including abundance, feeding habits and average life-span of infected mosquitoes, the mosquito species carrying the virus in sylvatic or urban settings, and preexisting immunity to the previous A226V strain in the human population (Coffey et al., 2013; Kilpatrick, 2011; Kilpatrick et al., 2006; Kuno and Chang, 2005; Le Flohic et al., 2013). Nevertheless, we showed the emergence of these variants in single mosquito infections in both primary mosquito vectors at a rate similar to that of the A226V epidemic strain. Fitness was more markedly increased in *Ae. albopictus*, the vector with a larger and expanding world distribution (Lambrechts et al., 2010). Furthermore, fitness was significantly increased in the small rodent model and in some human cell lines. These in vitro and in vivo phenotypes suggest that these mutations should at least be monitored over the years to come. In any case, such studies identify variants of biological significance that can help us better understand virus protein function and viral pathogenesis.

Finally, the conducted study focused on the E1 glycoprotein, which was previously implicated in the emergence of chikungunya epidemic variants. It will be interesting to further expand these studies to whole-genome sequencing of other circulating strain/mosquito combinations, since a number of new E2 glycoprotein mutations have been identified in recent Indian strains (Tsetsarkin and Weaver, 2011). Our approach is equally relevant to other arboviruses of clinical interest, such as dengue virus and West Nile virus. From a wider perspective of clinical and experimental host-pathogen studies, our results underscore the importance of monitoring virus evolution in specific subpopulations in vivo (e.g., salivary, fecal, seminal, and respiratory transmission samples), which may be missed at other sites. These studies provide an initial framework to understanding the temporal and spatial evolutionary trajectories of viruses as they disseminate through their host. We hope that such efforts could generate short lists of evolutionary intermediates most likely to emerge from a current strain to better target surveillance and ideally predict future emergence events in order to improve preparedness and response.

EXPERIMENTAL PROCEDURES

Cell and Viruses

Mammalian (BHK-21, Vero, and HeLa) cells were maintained in GlutaMAX Dulbecco's modified Eagle's medium (DMEM) supplemented with 10% newborn calf serum (NCS) (Gibco) and 1% penicillin and streptomycin (P/S) (Sigma-Aldrich) at 37°C with 5% CO_2. Human embryonic kidney 293T (HEK293T), NIH 3T3, Nor-10, A549, and BEAS-2B cells were maintained in DMEM supplemented with 10% fetal bovine serum (FBS) and 1% P/S. *Aedes albopictus* cells (C6/36 and U4.4) and *Aedes aegypti* cells (Aag-2) were maintained in L-15 Leibovitz medium supplemented with 10% FBS, 1% tryptose phosphate broth, 1% nonessential amino acids, and 1% P/S at 28°C. All cells were obtained from American Type Culture Collection (ATCC) and confirmed free of mycoplasma.

The viruses generated by reverse genetics were built on the infectious clone (Coffey and Vignuzzi, 2011) corresponding to chikungunya virus strain 06-049 (AM258994). The 2012 Cambodian patient isolate was obtained after

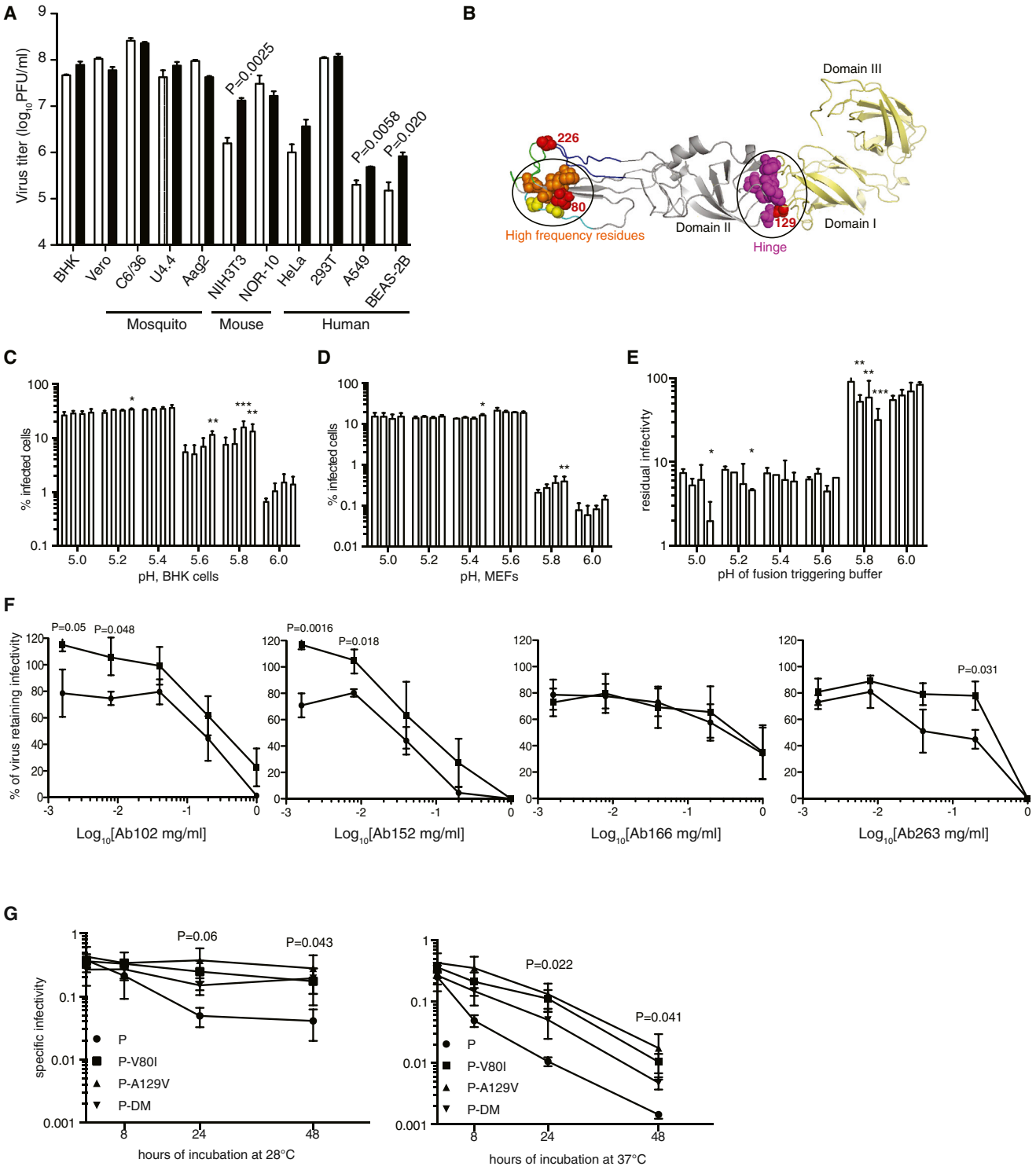

Figure 4. Molecular Modeling and In Vitro Studies Point to Increased Stability and Altered Fusogenic Activity of the P-DM Strain

(A) Progeny virus titers following infection of a panel of mammalian and mosquito cell lines with the parental A226V (open bars) or P-DM strain (solid bars). Mean values and SEM are shown. p values are indicated when significant; otherwise, differences between strains are not significant; n = 3; two-tailed unpaired t test. (B) GNM analysis of the E1 structure taken from the E1-E2 complex (PDB ID code: 2FXB) (Voss et al., 2010). Position 80 could be important for E1 structural stability or protein-protein interactions. Residue 80 (red) is in a cluster of the highest-frequency fluctuating residues (60, 64, 66, 80, 81, and 100–102; encircled and shown in atom spheres model). The cluster includes amino acids 64 and 66 (yellow) of the bc loop (cyan), which participates in E1 trimer-trimer interactions. Other structural elements of functional importance in the vicinity include the fusion (83–98, green), IJ (218–235, blue) loops, and position 226 (red). Amino acid 129 (red) is right near the main hinge of the protein (encircled); mutations in this position could affect E1's flexibility. The slowest mode of motion of E1 divides the structure

(legend continued on next page)

inoculation of a patient serum into C6/36 cells. Both stocks contain the A226V mutation that emerged during the 2005/2006 Indian Ocean outbreak. Infectious virus was produced by electroporating BHK cells with in vitro transcribed viral RNAs.

Virus Titrations and qRT-PCR

Virus titrations were determined by standard plaque assay on Vero cells. The limit of detection was 2.9 $\log_{10}$ pfu/ml. Viral RNA was isolated using TRIzol (Sigma-Aldrich) and measured with quantitative RT-PCR (qRT-PCR) using the Taqman RNA-to-C_T One-Step Quantitative RT-PCR kit (Applied Biosystems) as previously described (Coffey and Vignuzzi, 2011). BHK, C6/36, HEK293T, NIH 3T3, Nor-10, A549, and BEAS-2B cells were infected with each virus at a multiplicity of infection (moi) of 1. U4.4 and Aag2 cells were infected at moi = 10. Viral titers were determined by plaque assay.

Virus Binding Assays

BHK and C6/36 cells were incubated with CHIKV (moi = 5) at 4°C for the indicated times. At each time point, virus inoculum was removed, cells were washed three times with ice-cold PBS, and 500 μl of TRIzol was added for viral RNA extractions and qRT-PCR.

Lysosomotropic Agent Treatment

BHK and C6/36 cells were infected with virus at an moi of 5 in media containing Bafilomycin A1 for 16 hr. Following treatment, cells were fixed in 1% paraformaldehyde, and the number of GFP-expressing cells was quantified by flow cytometry.

Fusion from without Assay

BHK and MEF cells were preincubated in binding buffer at 4°C for 1 hr and then added to cells at an moi of 5 for 1 hr at 4°C. Unbound virus was removed and viral fusion was induced by adding prewarmed fusion buffer (RPMI, 10 mM HEPES, 2% BSA), adjusted to each pH described, for 2 min at 37°C. The pH was neutralized by the addition of complete media containing 20 mM NH_4Cl, and fusion was analyzed by flow cytometry.

Virus "Pretriggering" Assay

GFP-expressing viruses were preincubated in fusion buffer and adjusted to the indicated pH for 1 hr at 37°C. The pH was neutralized by the addition DMEM, and viral infectivity was measured by flow cytometry.

Virion Stability

Virus stocks were diluted to 10^5 pfu/ml in culture medium and incubated at 28°C or 37°C. At 0, 8, 24, and 48 hr, 100 μl aliquots were taken for titration of infectivity by plaque assay and for quantification of virus particles containing genomes by qRT-PCR. The specific infectivity was determined by dividing the infectious virus pfu values by the total number of genomes contained in the viral particles.

Fusion-Blocking Antibody Dynamics

Antibodies CHIK102, CHIK152, CHIK166, and CHIK263 were a kind gift from Michael Diamond (Pal et al., 2013). A total of 50 pfu of each virus was incubated at 4°C for 1 hr on a monolayer of Vero cells, and blocking antibodies were added for 1 hr at 4°C. To induce fusion, cells were incubated at 37°C for 15 min followed by the addition of an agarose overlay. Antibody inhibition was addressed 72 hr later.

Normal Mode Analysis

Normal mode analysis of E1 and the E1/E2 dimer was conducted using the Gaussian network model (GNM) (Emekli et al., 2008; Haliloglu et al., 1997) and the X-ray crystal structure of chikungunya virus particles E1-E2 (Protein Data Bank [PDB] ID code 2XFB) (Voss et al., 2010), where E1 is in complex with E2. GNM describes the protein structure as elastic network, in which the α carbon atoms within a cutoff radius are assumed to be connected by Hookean springs, displaying Gausssian fluctuations around their mean positions. The correlation between two nodes i and j, ΔR_i and ΔR_j, respectively, are calculated as $<\Delta R_i \Delta R_j> = (3k_BT/\gamma)[\Gamma^{-1}]_{ij} = (3k_BT/\gamma)\sum_k[\lambda_k{}^{-1}u_k u_k{}^T]_{ij}$, where Γ is an $N \times N$ Kirchhoff matrix of the internode contacts with the (commonly used) cutoff of 10 Å, where N is the number of amino acids in the protein. u_k and λ_k are the k-th eigenvectors and eigenvalues of Γ, k_B is the Boltzmann constant, T is the absolute temperature, and γ is a uniform force constant; k_BT/γ was taken as 1 $Å^2$. Overall, this equation predicts the mean-square displacement of each residue when $i = j$ and the correlations between the fluctuations of residues i and j when $i \neq j$, and when $i \neq j$, it predicts the correlations between the fluctuations of residues i and j as a superimposition of N-1 eigenmodes from the slowest to fastest modes of motion. Slow modes refer to cooperative and global motions, whereas fast modes refer to the residues displaying localized fast fluctuations. The results of the analysis of E1 alone and the E1/E2 complex are presented in Figures 4B and S3, respectively.

Mosquito Infections and Harvests

Aedes aegypti (1 lab-reared Rockefeller colony, 1 colony, F10 generation, collected in Bénoué, Cameroon in September 2007; 1 colony, F2 generations collected in Nakhon Chum, Thailand in 2011; 1 colony, F3 generations, collected in Kampong Cham, Cambodia) and *Aedes albopictus* (1 colony, F14 generation, collected in Bertoua, Cameroon in September 2007; 1 colony, F2 generations, collected in Phu Hoa, Vietnam in 2011) were used for mosquito infections. Viruses were diluted to 10^3 or 10^5 pfu/ml and mixed 1:2 with prewashed rabbit blood. Female mosquitoes were allowed to feed on 37°C blood meals through a chicken skin membrane for 20–60 min, after which engorged females were incubated at 28°C with 10% sucrose ad libitum; females that did not feed were excluded. Matched titers of blood meals (within 0.3 $\log_{10}$ pfu/ml) were verified by titrations of blood meals immediately after feeds. After incubations, legs and wings were removed, and the proboscis of each mosquito was inserted into a capillary tube containing 5 μl FBS for 45 min. Midguts, legs/wings, and salivary glands were dissected in PBS under 10× magnification. Saliva samples in FBS were added to 45 μl of L-15 media, and the legs/wings, bodies, and salivary glands were placed in 2 ml round bottom tubes

into two dynamic domains (gray and pale yellow), connected by a hinge region (residues 38, 128, 170, 256–259, and 267; magenta atom spheres model). See also Figure S3.

(C and D) After binding of GFP viruses onto cells, BHK cells (C) or MEFs (D) were treated with fusion buffer at a range of pH values (5.0–7.4). pH was then neutralized, and the amount of GFP-expressing cells was determined after 16 hr of infection. No significant differences were observed at pH values above 6.0 (not included in figure). Histograms are presented in the following order: parental P-GFP virus, P-V80I-GFP single mutation, P-A129V-GFP single mutation, and P-DM-GFP double mutation. The mean and SEM are shown; n = 3; *p < 0.05, **p < 0.01, ***p < 0.005; two-way ANOVA.

(E) GFP viruses were pretreated for 1 hr in cell-free fusion buffer at a range of pH to trigger fusion, and viruses for which fusion was not triggered were quantified by infecting BHK cells and measuring the percentage of GFP-positive cells. Histograms are presented in the following order: parental P-GFP virus, P-V80I-GFP single mutation, P-A129V-GFP single mutation, and P-DM-GFP double mutation. The mean and SEM are shown; n = 3; *p < 0.05, **p < 0.01, ***p < 0.005; two-way ANOVA.

(F) After binding to a monolayer of Vero cells, the parental (circle) or P-DM (square) strains were treated with serial dilutions of fusion-blocking antibodies, Ab102, Ab152, Ab166, and Ab263, and the ability to fuse was determined by measuring the percentage of virus retaining infectivity on Vero cells compared to untreated controls. n = 4; mean and SEM are shown; p values are indicated; two-tailed paired t test.

(G) Stability of viruses in cell-free environment at 28°C or 37°C. The parental (P), single mutants P-V80I and P-A129V, or double-mutant P-DM virus was incubated for 8, 24, and 48 hr in solution, and the residual specific infectivity was determined by plaque assay and qRT-PCR (n = 3; mean and SEM are shown; p values are shown for the variant that was closest to P strain in value; two-tailed paired t test).

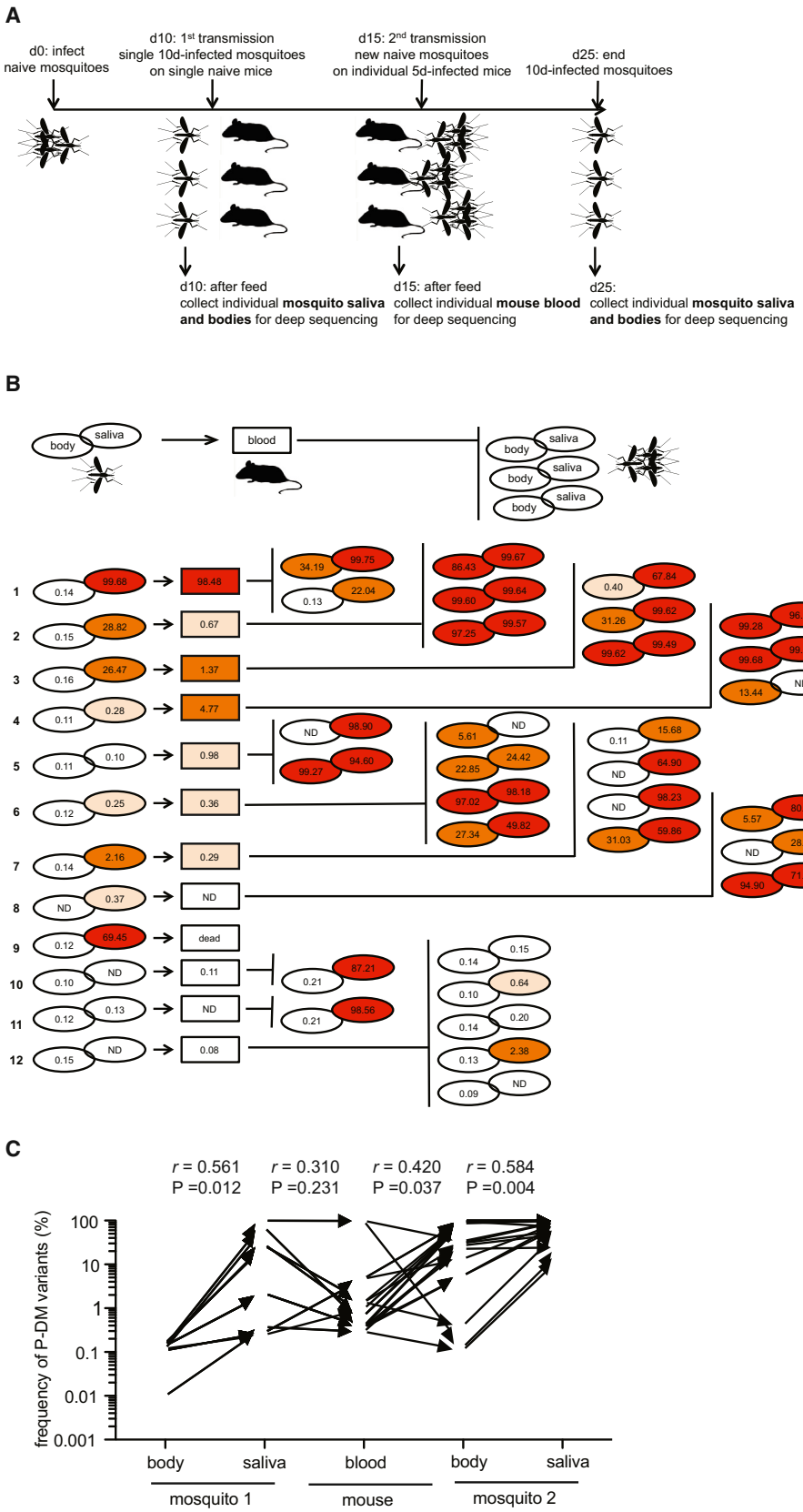

(legend on next page)

containing 300 μl DMEM and a steel ball. Samples were ground in a MM300 homogenizer (Retsch) at 30 shakes/s for 2 min. For infectivity determinations, whole bodies were ground individually, using the same homogenization methods. At least 20 mosquitoes were used per sample to ensure that enough mosquitoes fed and became positively infected for downstream analysis.

Mouse Infections

Mice were kept in the Pasteur Institute animal facilities in BSL-3 isolators, with water and food supplied ad libitum, handled in accordance with institutional guidelines for animal welfare, and at endpoint they were humanely euthanized complying with the Animal Committee regulations of Institut Pasteur in Paris, France, in accordance with the EC 86/609/CEE directive. C57B/6 mice (8 days old) were injected subcutaneously in the back with 200 pfu of virus, and at selected times postinoculation, animals were sacrificed and blood and organs were harvested. Organs were placed individually in tubes and homogenized as for mosquitoes. Survival curves were generated by injecting 8-day- or 3-week-old female mice with 10^6 pfu of virus and monitoring morbidity and mortality for 14 days after infection.

Transmission Studies

Transmission experiments were conducted at the Institut Pasteur in Cambodia in Phnom Penh in BSL3 facilities. Briefly, mosquitoes were infected as described previously and incubated at 28°C for 10 days. On day 10, individual mosquitoes were allowed to feed on individual 5-day-old Swiss mice until engorged. Swiss mice (5 days old) were immobilized on a mesh surface suspended over a cup containing an individual mosquito at 28°C. Mice and mosquitoes were incubated together for 1 hr or until feeding had occurred. Following feeding, mice were returned to cages, and individual mosquitoes were salivated and their bodies crushed and harvested. Mice were monitored for disease for 5 days. After 5 days of infection in mice, naive mosquitoes were allowed to feed on individual infected mice until engorged. Following feeding, mice were sacrificed and blood was harvested. These mosquitoes were then incubated at 28°C for ten days, salivated and their bodies crushed and harvested. Amplicons for deep sequencing were prepared immediately after harvesting in vivo samples, which improved the overall yield compared to using frozen samples.

High-Throughput Sanger Sequencing and Genetic Diversity

For genetic diversity and bottleneck experiments, amplicons flanking the partial E1 gene were generated using the Titan one-step RT-PCR kit (Roche) and primers flanking genome positions 9,943–10,746. Amplicons were cloned into TOPO vectors (Invitrogen) and sequenced using Sanger technology in 96-well format (GATC Biotech). Mutation frequencies were determined by dividing the number of nucleotide polymorphisms in all clones (where polymorphisms at the same genetic locus on multiple clones were counted once) by the number of nucleotides sequenced. Values were then represented as the number of mutations per 10^4 nt sequenced.

Deep Sequencing of Samples

Viral RNAs were isolated from samples by TRIzol extraction, and the E1 gene was amplified using the Titan one-step RT-PCR kit (Roche) with the primers E1Forward(9943) 5′-TACGAACACGTAACAGTGATCC-3′ and E1Reverse(10726) 5′-CGCTCTTACCGGGTTTGTTG-3′ following manufacturer's instructions. PCR fragments were purified via the NucleoSpin Gel and PCR Clean-up kit (Macherey-Nagel), and total DNA was quantified by NanoDrop. PCR products were then fragmented (Fragmentase), linked to Illumina multiplex adapters, clusterized, and sequenced with Illumina cBot and GAIIX technology. Sequences were demultiplexed using Illumina's CASAVA software, allowing for no mismatches in the multiplex tag sequences. Quality filtering (95%–98% of reads passed) and adaptor cleaning were done using fastq-clipper (http://hannonlab.cshl.edu/fastx_toolkit/index.html). The 75 nt reads were aligned to the E1 sequence as a reference, with a maximum two mismatches per read using BWA (Li and Durbin, 2009). Alignments were processed using SAMTOOLS (Li et al., 2009) to obtain the nucleotide/base calling at each position. An in-house ViVAn (virus variance analysis) pipeline was used to identify statistically significant variants above the background noise due to sequencing error calculated for each nucleotide site. Briefly, for each position throughout the viral genome, base identity and their quality scores were gathered. Each variant allele's rate was initially modified according to its covering read qualities based on a maximum likelihood estimation and tested for significance using a generalized likelihood-ratio test. Additionally, an allele confidence interval was calculated for each allele. In order to correct for multiple testing, a Benjamini-Hochberg false discovery rate of 5% was set. In all experiments, a minimum coverage of 25,000 reads was obtained, and the background error at every nucleotide site was always below 0.01%.

Statistical Analyses

No samples or infected animals were excluded from analysis. Animals were randomly allocated to groups before infections were performed. No blinding was performed during experimentation and analysis. All statistical tests (described in each figure legend) were conducted using GraphPad Prism software. p values > 0.05 were considered nonsignificant (ns).

SUPPLEMENTAL INFORMATION

Supplemental Information includes Supplemental Experimental Procedures, five figures, and one table and can be found with this article online at http://dx.doi.org/10.1016/j.chom.2014.05.008.

ACKNOWLEDGMENTS

This work was supported by the European Research Council (ERC Starting Grant No. 242719), by the Bill and Melinda Gates Foundation Grand Challenges Exploration Initiative, the French Government's Investissement d'Avenir program, Laboratoire d'Excellence "Integrative Biology of Emerging Infectious Diseases" (grant ANR-10-LABX-62-IBEID), and the Israel-France High Council for Science and Technology Research "Complexity in Biology" program. Salary for L.L.C. and K.A.S. was provided by the Region of Ile-de-France DIM program on Infectious, Parasitic or Nosocomial Emerging Diseases and the Philippe Foundation. Salary for A.V.B. was supported by the French National grant ANR-09-JCJC-0118-1. Salary for C.A.-G. was supported by the French Ministry of Superior Education and Research. N.B.-T.

Figure 5. Emergence of V80I:A129V E1 Glycoprotein Variants during Insect-Mammal-Insect Transmission

(A) Mosquitoes were fed blood meals containing the parental A226V strain (d0), and infection was allowed to proceed for 10 days (d10). Individual mosquitoes were then separated and allowed to feed on individual naive mice, after which their saliva and bodies were harvested for deep sequencing. Mice exposed to infected mosquitoes were incubated for 5 days (d15), upon which time new batches of several mosquitoes were allowed to feed on individual mice. Mouse blood was then harvested for deep sequencing. The infection of the second set of mosquitoes was incubated for another 10 days (d25), at which point their bodies and saliva were harvested for deep sequencing.

(B) Deep sequencing analysis of individual mosquito body, saliva, and mouse blood samples. The bubble diagrams illustrate each mosquito-to-mouse-to-multiple mosquitoes transmission series for the 12 mosquitoes initially infected with A226V strain that successfully transmitted to mice. The numbers within the bubbles indicate the percentage of the V80I:A129V mutations in each virus subpopulation. Both variants were present at the same frequency and confirmed to be linked on the same genomes by Sanger sequencing of plaque-purified virus. The background limit of detection was <0.01%; light shading represents >0.2%; medium shading represents >1.0%; dark shading represents >50%. ND, virus confirmed present, but not determined due to inability to obtain suitable amplicons for deep sequencing. Dead, mouse succumbed to infection before transmission was performed. See also Figure S5.

(C) Dynamics of V80I:A129V mutation frequency during transmission. Arrows represent the increase or decrease of variant frequency (percentage of total virus subpopulation) for each matched body → saliva → blood → body → saliva transmission series in (A). The correlation, *r*, and p values are shown; Spearman's two-tailed correlation coefficient and permutation test.

and T.H. were supported by NATO traveling grant CBP.MD.CLG 984340. We are grateful to Ngan Chantha, Huy Rekol, and the team of the National Malaria Centre in Cambodia for providing clinical specimens. We thank Christophe Paupy (IRD), Louis Lambrechts, and Paul Reiter (IP) for providing some mosquito strains.

Received: December 19, 2013
Revised: March 19, 2014
Accepted: April 22, 2014
Published: June 11, 2014

REFERENCES

Ciota, A.T., Ehrbar, D.J., Van Slyke, G.A., Payne, A.F., Willsey, G.G., Viscio, R.E., and Kramer, L.D. (2012). Quantification of intrahost bottlenecks of West Nile virus in Culex pipiens mosquitoes using an artificial mutant swarm. Infect. Genet. Evol. *12*, 557–564.

Coffey, L.L., and Vignuzzi, M. (2011). Host alternation of chikungunya virus increases fitness while restricting population diversity and adaptability to novel selective pressures. J. Virol. *85*, 1025–1035.

Coffey, L.L., Forrester, N., Tsetsarkin, K., Vasilakis, N., and Weaver, S.C. (2013). Factors shaping the adaptive landscape for arboviruses: implications for the emergence of disease. Future Microbiol. *8*, 155–176.

Couderc, T., Chrétien, F., Schilte, C., Disson, O., Brigitte, M., Guivel-Benhassine, F., Touret, Y., Barau, G., Cayet, N., Schuffenecker, I., et al. (2008). A mouse model for Chikungunya: young age and inefficient type-I interferon signaling are risk factors for severe disease. PLoS Pathog. *4*, e29.

Davis, C.T., Ebel, G.D., Lanciotti, R.S., Brault, A.C., Guzman, H., Siirin, M., Lambert, A., Parsons, R.E., Beasley, D.W.C., Novak, R.J., et al. (2005). Phylogenetic analysis of North American West Nile virus isolates, 2001-2004: evidence for the emergence of a dominant genotype. Virology *342*, 252–265.

Domingo, E. (2010). Mechanisms of viral emergence. Vet. Res. *41*, 38.

Emekli, U., Schneidman-Duhovny, D., Wolfson, H.J., Nussinov, R., and Haliloglu, T. (2008). HingeProt: automated prediction of hinges in protein structures. Proteins *70*, 1219–1227.

Forrester, N.L., Guerbois, M., Seymour, R.L., Spratt, H., and Weaver, S.C. (2012). Vector-borne transmission imposes a severe bottleneck on an RNA virus population. PLoS Pathog. *8*, e1002897.

Haliloglu, T., Bahar, I., and Erman, B. (1997). Gaussian dynamics of folded proteins. Phys. Rev. Lett. *79*, 3090–3093.

Herfst, S., Schrauwen, E.J.A., Linster, M., Chutinimitkul, S., de Wit, E., Munster, V.J., Sorrell, E.M., Bestebroer, T.M., Burke, D.F., Smith, D.J., et al. (2012). Airborne transmission of influenza A/H5N1 virus between ferrets. Science *336*, 1534–1541.

Holmes, E.C. (2013). What can we predict about viral evolution and emergence? Curr Opin Virol *3*, 180–184.

Imai, M., Watanabe, T., Hatta, M., Das, S.C., Ozawa, M., Shinya, K., Zhong, G., Hanson, A., Katsura, H., Watanabe, S., et al. (2012). Experimental adaptation of an influenza H5 HA confers respiratory droplet transmission to a reassortant H5 HA/H1N1 virus in ferrets. Nature *486*, 420–428.

Kilpatrick, A.M. (2011). Globalization, land use, and the invasion of West Nile virus. Science *334*, 323–327.

Kilpatrick, A.M., Daszak, P., Goodman, S.J., Rogg, H., Kramer, L.D., Cedeño, V., and Cunningham, A.A. (2006). Predicting pathogen introduction: West Nile virus spread to Galáipagos. Conserv. Biol. *20*, 1224–1231.

Kuno, G., and Chang, G.-J.J. (2005). Biological transmission of arboviruses: reexamination of and new insights into components, mechanisms, and unique traits as well as their evolutionary trends. Clin. Microbiol. Rev. *18*, 608–637.

Lambrechts, L., Scott, T.W., and Gubler, D.J. (2010). Consequences of the expanding global distribution of Aedes albopictus for dengue virus transmission. PLoS Negl. Trop. Dis. *4*, e646.

Le Flohic, G., Porphyre, V., Barbazan, P., and Gonzalez, J.P. (2013). Review of climate, landscape, and viral genetics as drivers of the Japanese encephalitis virus ecology. PLoS Negl. Trop. Dis. *7*, e2208.

Li, H., and Durbin, R. (2009). Fast and accurate short read alignment with Burrows-Wheeler transform. Bioinformatics *25*, 1754–1760.

Li, H., Handsaker, B., Wysoker, A., Fennell, T., Ruan, J., Homer, N., Marth, G., Abecasis, G., and Durbin, R.; 1000 Genome Project Data Processing Subgroup (2009). The Sequence Alignment/Map format and SAMtools. Bioinformatics *25*, 2078–2079.

Manimunda, S.P., Mavalankar, D., Bandyopadhyay, T., and Sugunan, A.P. (2011). Chikungunya epidemic-related mortality. Epidemiol. Infect. *139*, 1410–1412.

Ozden, S., Huerre, M., Riviere, J.-P., Coffey, L.L., Afonso, P.V., Mouly, V., de Monredon, J., Roger, J.-C., El Amrani, M., Yvin, J.L., et al. (2007). Human muscle satellite cells as targets of Chikungunya virus infection. PLoS ONE *2*, e527.

Pal, P., Dowd, K.A., Brien, J.D., Edeling, M.A., Gorlatov, S., Johnson, S., Lee, I., Akahata, W., Nabel, G.J., Richter, M.K.S., et al. (2013). Development of a highly protective combination monoclonal antibody therapy against Chikungunya virus. PLoS Pathog. *9*, e1003312.

Renault, P., Josseran, L., and Pierre, V. (2008). Chikungunya-related fatality rates, Mauritius, India, and Reunion Island. Emerg. Infect. Dis. *14*, 1327.

Schuffenecker, I., Iteman, I., Michault, A., Murri, S., Frangeul, L., Vaney, M.-C., Lavenir, R., Pardigon, N., Reynes, J.-M., Pettinelli, F., et al. (2006). Genome microevolution of chikungunya viruses causing the Indian Ocean outbreak. PLoS Med. *3*, e263.

Tsetsarkin, K.A., and Weaver, S.C. (2011). Sequential adaptive mutations enhance efficient vector switching by Chikungunya virus and its epidemic emergence. PLoS Pathog. *7*, e1002412.

Tsetsarkin, K.A., Vanlandingham, D.L., McGee, C.E., and Higgs, S. (2007). A single mutation in chikungunya virus affects vector specificity and epidemic potential. PLoS Pathog. *3*, e201.

Tsetsarkin, K.A., Chen, R., Leal, G., Forrester, N., Higgs, S., Huang, J., and Weaver, S.C. (2011). Chikungunya virus emergence is constrained in Asia by lineage-specific adaptive landscapes. Proc. Natl. Acad. Sci. USA *108*, 7872–7877.

Vazeille, M., Moutailler, S., Coudrier, D., Rousseaux, C., Khun, H., Huerre, M., Thiria, J., Dehecq, J.-S., Fontenille, D., Schuffenecker, I., et al. (2007). Two Chikungunya isolates from the outbreak of La Reunion (Indian Ocean) exhibit different patterns of infection in the mosquito, Aedes albopictus. PLoS ONE *2*, e1168.

Voss, J.E., Vaney, M.-C., Duquerroy, S., Vonrhein, C., Girard-Blanc, C., Crublet, E., Thompson, A., Bricogne, G., and Rey, F.A. (2010). Glycoprotein organization of Chikungunya virus particles revealed by X-ray crystallography. Nature *468*, 709–712.

Weaver, S.C., and Barrett, A.D.T. (2004). Transmission cycles, host range, evolution and emergence of arboviral disease. Nat. Rev. Microbiol. *2*, 789–801.

Ziegler, S.A., Lu, L., da Rosa, A.P.A.T., Xiao, S.-Y., and Tesh, R.B. (2008). An animal model for studying the pathogenesis of chikungunya virus infection. Am. J. Trop. Med. Hyg. *79*, 133–139.

Cell Host & Microbe, Volume *15*

Supplemental Information

Emergence and Transmission of Arbovirus Evolutionary Intermediates with Epidemic Potential

Kenneth A. Stapleford, Lark L. Coffey, Sreyrath Lay, Antonio V. Bordería, Veasna Duong, Ofer Isakov, Kathryn Rozen-Gagnon, Camilo Arias-Goeta, Hervé Blanc, Stéphanie Beaucourt, Türkan Haliloğlu, Christine Schmitt, Isabelle Bonne, Nir Ben-Tal, Noam Shomron, Anna-Bella Failloux, Philippe Buchy, and Marco Vignuzzi

Supplemental Information

Figure S1, related to Figure 4. A-B, Binding efficiency of viruses in mammalian BHK (**A**) and mosquito C6/36 (**B**) cells. The parental A226V (P), single mutant P-V80I or P-A129V, or the double mutant P-DM viruses were allowed to bind for the indicated times at 4°C, cells were washed extensively with cold PBS followed by the addition of Trizol and bound virus was quantified by qRT-PCR (n=3, mean and S.E.M. are shown, no significant differences observed, two-tailed unpaired t test). **C-D,** pH dependence of GFP-expressing virus entry in BHK (**C**) or C6/36 (**D**) cells at 16h of infection, following treatment with different concentrations of Bafilomycin A1. The percentage of infected cells was determined by GFP-expression (n=3, mean and S.E.M. are shown, no significant differences observed, two-tailed unpaired t test). **E-H,** One-step viral growth kinetics in mammalian BHK (**E,G**) or mosquito C6/36 (**F, H**) cells. Cells were infected at MOI=1 and at indicated times, infectious progeny was assayed by plaque assay (**E**, **F**) and viral RNA levels were quantified by qRT-PCR (**G**, **H**). n=3, mean and S.E.M are shown, no significant differences were observed, two-tailed unpaired t test. **I,** Expression of glycoproteins by parental A226V (P) or P-DM in BHK cells, the presumed identities of the peptides base on molecular weight are indicated.

Figure S2, related to Figure 4. Electron microscopy reveals no significant differences in virus and cell morphology. A,B, Scanning electron microscopy of parental A226V (**A**) and P-DM (**B**) infected C6/36 mosquito cells showing characteristic budding of chikungunya virus. **C,D,** Transmission electron microscopy of parental A226V (**C**) and P-DM (**D**) infected C6/36 cells revealing similar cell morphology, virus morphology and budding (black arrowheads). **E,F,** Transmission

electron microscopy of parental A226V (**E**) and P-DM (**F**) infected human HeLa cells reveal no significant differences in cell morphology and virus morphology and budding (black arrowheads). **G,H,** Negative-stain transmission electron microscopy of purified A226V (**G**) and P-DM (**H**) virion reveal no significant differences in virus morphology.

Figure S3, related to Figure 4B. Importance of positions 80 and 129 for E1 structural dynamics and function. Normal mode analysis of E1 was conducted using the Gaussian Network Model (GNM)(Emekli et al., 2008; Haliloglu et al., 1997) and the X-ray crystal structure of Chikungunya virus particles E1-E2 (PDB code: 2XFB)(Voss et al., 2010). The E1 molecule is presented using dark colors (orange and grey) and E2 with pale colors (yellow and light grey). The second slowest mode, shown here, divides the dimer into three dynamic domains: The left-most domain, marked with orange (E1) and yellow (E2), the central domain, marked with grey (E1) and light grey (E2), and the right-most, marked with orange (E1). Two hinge regions, marked in magenta, connect the dynamic domains. The left hinge includes positions 52, 108, 214 and 236 of E1, and 72, 74, 77, 231 and 317 of E2. The right hinge includes positions 10, 34, 131, 146, 150, 163, 277, 384 and 389 of E1. The fusion and IJ loops on E1 are shown in green and blue, respectively. Positions 80, 129 and 226 of E1 are highlighted in red. **The V80I mutation,** valine 80 is in a cluster of residues that fluctuate in the fastest mode of E1, implying its function importance. The cluster that includes residues 60, 64, 66, 80, 81 and 100-102 could be important for the structural stability of E1 and also for its interactions with other protein molecules. The cluster is in a 'hot region' of the protein, in the vicinity to the fusion (83-98) and ij (218-235) loops. Specifically, residue 60 of the cluster is in

direct contact with residues 84, 86, 93, 94 and 98 of the fusion loop, and residues 80 and 81 of the cluster are in direct contact with residues 221-224 of the ij loop. Both loops undergo conformation changes. At neutral pH a conformation in which the fusion peptide is buried in a pocket in the E2 protein is assumed. However, in the acidic pH of the endosome E1 detaches from E2, and the ij and fusion loops undergo conformational change that exposes the fusion loop, making it prone to interact with the endosome membrane. The cluster could be involved in the control of this key conformational change and the V80I mutation could alter characteristics of the transition (e.g., affect the relative stability of the two conformations and/or the transition rate). Furthermore, the high frequency cluster also contains residues 64 and 66 of the bc loop of domain II, a mediator of the interaction between two E1 trimers in the so called "contact 2" region described in the E1-E1 interactions of the fusion protein of Semliki Forest virus(Gibbons et al., 2004). In particular, contact 2 involves interactions of residues 63-69 of the bc loop of one of the E1 trimers with residues 89–92 (part of the fusion loop) of the neighboring trimer. Residue 80 is at the core of the cluster, and the V80I mutation could affect the contact 2 region of the E1 trimer interface, which is known to be important in the early step of membrane fusion. **The A129V mutation,** alanine 129 is at the interface between domains I and II of E1, a major hinge region, controlling the inter-domain motion and the relative positioning of the domains in the protein. The alanine-to-valine mutation could therefore affect the internal conformation of E1 as well as conformational changes. Position 129 is also close to a main hinge in the dynamics of the E1-E2 dimer and the mutation could affect the flexibility and functional dynamics of the protein complex. Analysis of the slowest modes of motion of the E1 trimer structure (PDB ID: 1RER), corresponding to the low pH, fusion prone, conformation of the protein, shows that position 129 is a

hinge and position 80 is near a hinge (data not shown). This is further evidence for the importance of these positions for the dynamics and conformational changes.

Figure S4, related to Figure 5. Schematic of V80I:A129V:A226V emergence during transmission. The relative frequencies of the V80I:A129V mutations during infection and transmission suggest that the variants are first generated at low frequency in the tissues of the mosquito (body, mosquito 1), and accumulate to approximately 10-fold higher frequencies than in the original virus stock (indicated by star). The similar fitness of these variants compared to wild type in most tissues could account for the lack of substantially rapid selection within mosquito tissue itself. The first significant increase in frequency occurs in the cell-free saliva, where the variants are deposited and accumulate by maintaining structural integrity and infectivity with respect to the original parental strain (saliva, mosquito 1). The presence of these variants is maintained during passage in mammals (blood, mouse), although the increase or decrease in frequency appears to be stochastic and may depend on founder effects of which genotypes are first to replicate within the mammal. When present in mammals, transmission to mosquitoes results in a significant amplification of these variants in mosquito tissue, possibly aided by improved fusogenic activity (body, mosquito 2), followed by further amplification in saliva, where the V80I:A129V mutations become fixed to the majority genotype.

Figure S5, related to Figure 5. Emergence and transmission of V80I:A129V mutations in Asian mosquitoes. Mosquitoes were presented blood meals containing chikungunya A226V virus (d0) and infection was allowed to proceed for 10 days (d10). Individual mosquitoes were then separated and allowed to feed on individual

naïve mice, after which their saliva and bodies were harvested for deep sequencing. Mice exposed to infected mosquitoes were incubated for 5 days (d15), upon which time new batches of several mosquitoes were allowed to feed on individual mice. Mouse blood was then harvested for deep sequencing. The infection of the second set of mosquitoes was incubated for another 10 days (d25), at which points their bodies and saliva were harvested for deep sequencing. Deep sequence analysis of individual mosquito body, saliva and mouse blood samples are shown and represented in oval diagrams. The numbers indicate the percentage of the V80I:A129V mutations in each virus subpopulation. The background limit of detection was <0.01%, light shading represents >0.2%, medium shading >1.0% and dark shading >50%. ND, virus confirmed present, but not determined due to inability to obtain suitable amplicons for deep sequencing.

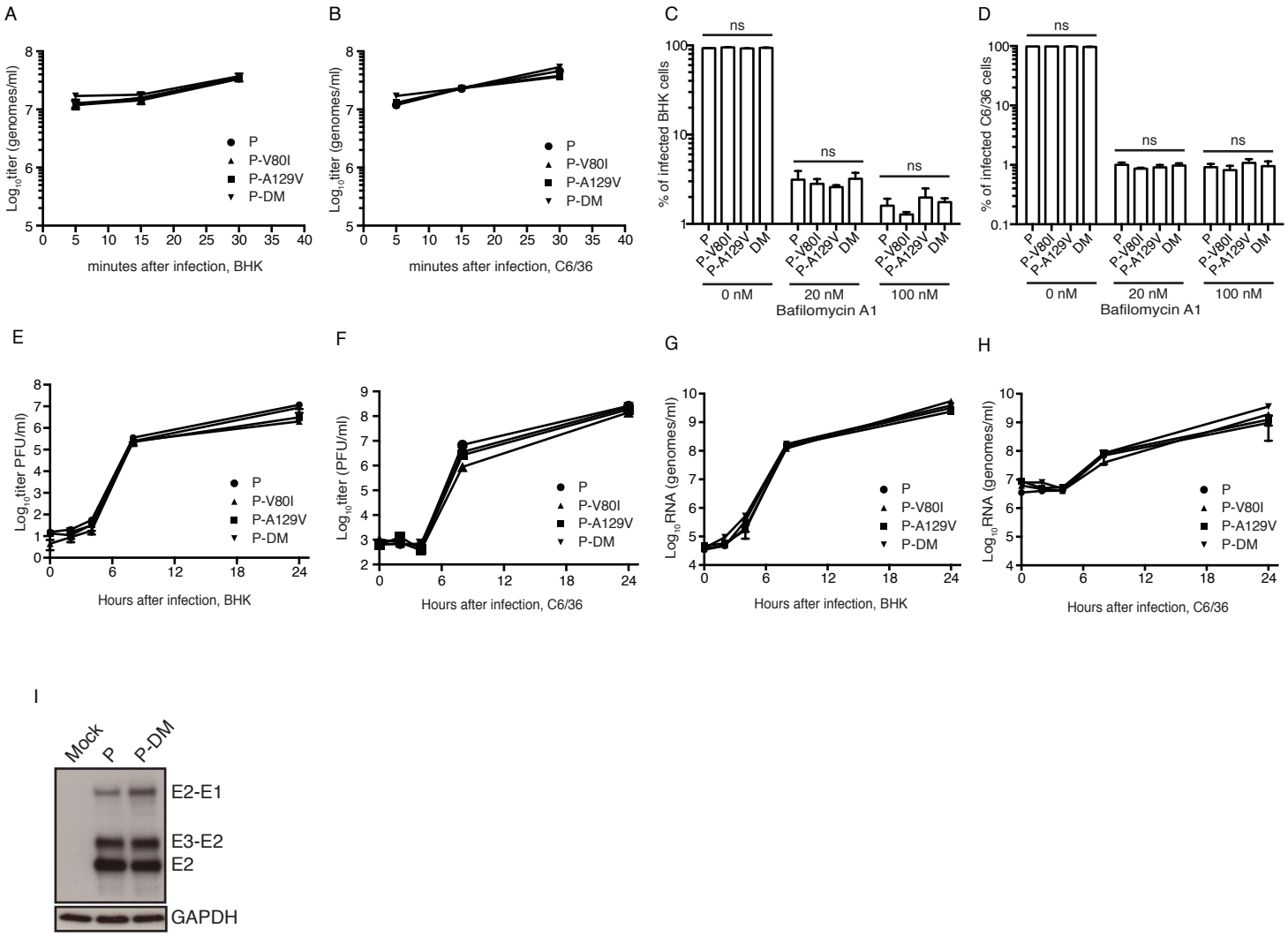
A
B
C
D
E
F
G
H
I
Log10titer (genomes/ml)
minutes after infection, BHK
minutes after infection, C6/36
P
P-V80I
P-A129V
P-DM
% of infected BHK cells
% of infected C6/36 cells
ns
0 nM
20 nM
100 nM
Bafilomycin A1
Log10titer PFU/ml)
Log10titer (PFU/ml)
Hours after infection, BHK
Hours after infection, C6/36
Log10RNA (genomes/ml)
Mock
E2-E1
E3-E2
E2
GAPDH

A

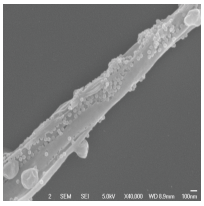

B

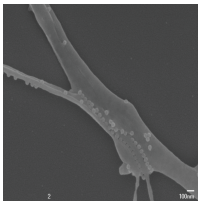

C

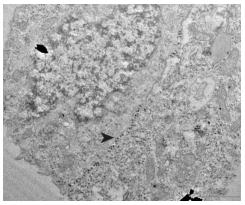

D

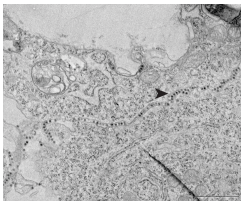

E

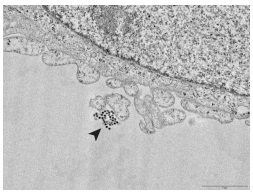

F

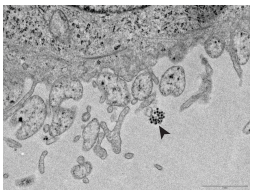

G

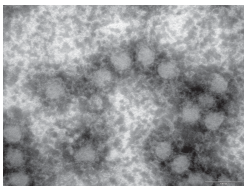

H

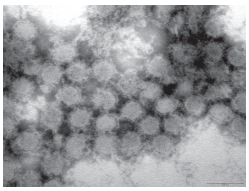

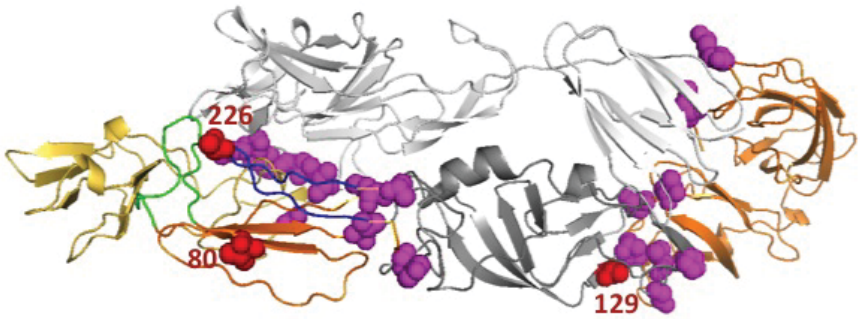
226
80
129

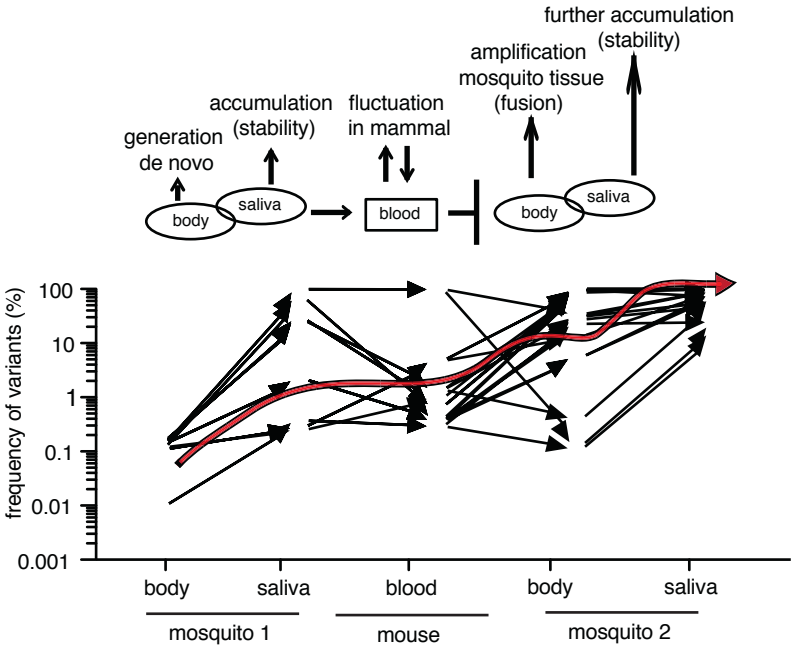
further accumulation
(stability)
amplification
mosquito tissue
(fusion)
accumulation
(stability)
fluctuation
in mammal
generation
de novo
body
saliva
blood
body
saliva
frequency of variants (%)
100
10
1
0.1
0.01
0.001
body
saliva
blood
body
saliva
mosquito 1
mouse
mosquito 2

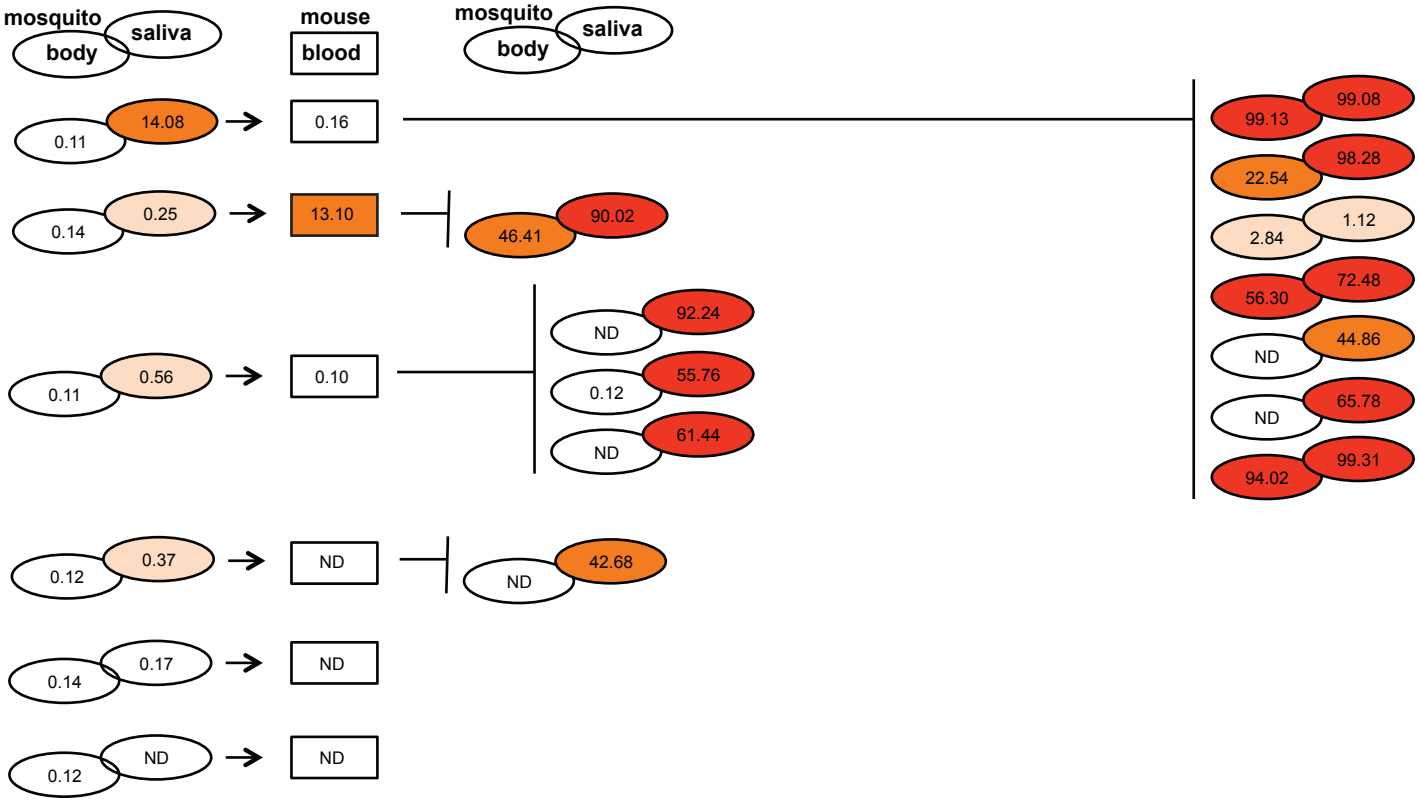
mosquito
body
saliva
mouse
blood
mosquito
body
saliva
0.11
14.08
0.16
99.13
99.08
22.54
98.28
2.84
1.12
56.30
72.48
ND
44.86
ND
65.78
94.02
99.31
0.14
0.25
13.10
46.41
90.02
0.11
0.56
0.10
ND
92.24
0.12
55.76
ND
61.44
0.12
0.37
ND
ND
42.68
0.14
0.17
ND
0.12
ND
ND

Experimental Procedures

Cells

Mammalian (BHK-21, Vero and HeLa) cells were maintained in GlutaMAX^{TM} Dulbecco's Modified Eagle Medium (DMEM) supplemented with 10% new-born calf serum (NCS) (Gibco) and 1% penicillin and streptomycin (P/S) (Sigma-Aldrich) at 37ºC with 5% CO_2. HEK293T, NIH3T3, Nor-10, A549, and BEAS-2B cells were maintained in DMEM supplemented with 10% fetal-bovine serum (FBS) and 1% P/S. *Aedes albopictus* cells (C6/36 and U4.4) and *Aedes aegypti* cells (Aag-2) were maintained in L-15 Leibovitz medium supplemented with 10% FBS, 1% tryptose phosphate broth, 1% nonessential amino acids, and 1% P/S at 28ºC. All cells were obtained from ATCC and confirmed free of mycoplasma.

Viruses

The infectious clone(Coffey and Vignuzzi, 2011) used to generate virus stocks in this study corresponds to chikungunya virus strain 06-049 (AM258994). To generate an isogenic chikungunya GFP-expressing infectious clone, the AgeI/XhoI restriction fragment of a previously purchased GFP-expressing infectious clone derived from chikungunya virus LR2006 (European Virus Archive) was inserted into the same restriction sites of the infectious clone described above. The 2012 Cambodian patient isolate was obtained after inoculation of a patient serum into C6/36 cells. The patient's blood sample was collected for diagnostic purposes by the National Centre for Malariology, Ministry of Health in Cambodia, during an outbreak investigation (which does not require prior approval from National Ethics Committee). The patient's sample and the virus strain were then anonymized for the purpose of this study. Both stocks contain the A226V mutation that emerged during the 2005/2006 Indian Ocean outbreak. The newly identified E1 mutations, V80I and A129V, were

introduced into the A226V infectious clone backbones using Quikchange II XL site-directed mutagenesis (Agilent) following the manufacturer's instructions. To study the pre-2005/2006 epidemic strain, residue 226V was reverted to the original A226 in a separate construct. The following primers were used to generate each mutation (in bold): V80I Forward 5' CCTGACTACAGCTGTAAG**A**TCTTCACCGGCGTCTACCC 3', V80IReverse 5' GGGTAGACGCCGGTGAAGA**T**CTTACAGCTGTAGTCAGG 3', A129V Forward 5' CAGGGCTCATACCGCATCTG**T**ATCAGCTAAGCTCCGCGTC 3', and A129V Reverse 5' GACGCGGAGCTTAGCTGAT**A**CAGATGCGGTATGAGCCCTG 3', V226AForward 5' CTGCAGAGACCGGCTG**C**GGGTACGGTACACGTG 3', and V226AReverse 5' CACGTGTACCGTACCC**G**CAGCCGGTCTCTGCAG 3'. 10 µg of each plasmid was linearized overnight with *NotI* followed by two phenol:chloroform extractions and an ethanol precipitation. Plasmids were resuspended in nuclease-free water at 1 µg/µl. *In vitro* transcribed viral RNAs were produced from linearized plasmids using the SP6 mMESSAGE mMACHINE kit (Ambion) following the manufacturer's instructions. After RNA synthesis, samples were DNase treated and RNAs were purified by phenol:chloroform extraction, ethanol precipitation, and resuspended at a concentration of 1 µg/µl. All RNAs were stored at -80ºC until electroporation. Infectious virus was produced by electroporating BHK cells with *in vitro* transcribed viral RNAs. BHK cells were trypsinized, washed twice with ice-cold PBS, and resuspended at $2x10^7$ cells/ml in PBS. 390 µl of cells were mixed with 10 µl (10 µg) of *in vitro* transcribed RNA and added to a 2 mm electroporation cuvette. Cells were electroporated with 2 pulses at 1.2 kV, 25 F, with infinite resistance in a XCell Gene Pulser (BioRad). Cells were allowed to recover for 10 min at room temperature, transferred into 6 ml of warm DMEM, and placed in a T25 flask at 37ºC for 48 h. Virus was harvested, spun at 1,200 x g for 5 min to remove debris, and viral titers were determined by plaque assay.

Virus titrations

For plaque assays, 10-fold serial dilutions of virus were made in DMEM and each dilution was incubated on a Vero monolayer for 1 h. Following incubations, a 0.8% agarose overlay was added containing DMEM with 2% NCS, and plaques were allowed to develop for 72 h. Cells and virus were then fixed with 4% formalin, the agarose plugs were removed, and plaques were visualized by staining with crystal violet (10% crystal violet with 20% ethanol in H_2O). Titers were recorded as the reciprocal of the highest dilution where plaques were noted. The limit of detection was 2.9 log10 PFU/ml.

Viral RNA extractions and qRT-PCR

Viral RNA was isolated using TRIzol (Sigma-Aldrich) following manufacturer's instructions. Viral RNA concentrations were measured with qRT-PCR using the Taqman RNA-to-C_T one-step quantitative RT-PCR kit (Applied Biosystems) as previously described(Coffey and Vignuzzi, 2011). A standard curve was generated for each data set from duplicate replicates of *in vitro* transcribed RNAs.

Virus binding assays

BHK and C6/36 cells were incubated with CHIKV (MOI=5) at 4°C for the indicated times. At each time point, virus inoculum was removed, cells were washed three times with ice-cold PBS, and 500 µl of TRIzol was added for viral RNA extractions and qRT-PCR.

Lysosomotropic agent treatment

BHK and C6/36 cells were pre-incubated in media containing 0, 20 or 100 nM of Bafilomycin A1 for 1 h. Virus was diluted to an MOI of 5 in DMEM containing each inhibitor and added to cells for 1 h. Cells were washed extensively with PBS and media containing Bafilomycin A1 was added for 16 h. Following treatment, supernatants were removed, cells washed with PBS, trypsinized, and fixed in 1% paraformaldehyde (PFA). The number of GFP-expressing cells was quantified by flow cytometry.

Fusion from without assay

BHK and MEF cells were chilled at 4°C and pre-incubated in binding buffer (RPMI, 10 mM HEPES, 2% bovine serum albumin (BSA), 20 mM NH_4Cl, pH 7.4) for 1 h. Each virus was diluted in binding buffer and added to cells at an MOI of 5 for 1 h at 4°C. Unbound virus was removed and viral fusion was induced by the addition of pre-warmed fusion buffer (RPMI, 10 mM HEPES, 2% BSA) adjusted to each pH described for 2 min at 37°C. The pH was neutralized by the addition of complete media containing 20 mM NH_4Cl and fusion was analyzed by flow cytometry.

Virus "pre-triggering" assay

To address the role of pH prior to membrane binding, GFP-expressing viruses were preincubated in fusion buffer (RPMI, 10 mM HEPES, 2% BSA) adjusted to the indicated pH for 1 h at 37ºC. The pH was neutralized by the addition DMEM and viral infectivity was measured by flow cytometry.

Growth curves and RNA synthesis

One-step viral growth curves were performed in triplicate by infecting BHK and C6/36 cells with each virus variant at an MOI = 1 for 1 h. Cells were washed 3 times with 1X PBS to remove unbound virus and fresh media was added. Supernatant aliquots were taken at each time point and an equal volume of fresh media was added back to compensate for removed volume. U4.4 and Aag2 cells were infected at MOI = 10 and progeny virus was tittered from supernatant 24 h after infection. HEK293T, NIH3T3, Nor-10, A549, and BEAS-2B cells were infected at an MOI = 1 and progeny virus was titrated from supernatants 24 h after infection. Viral titers were determined by plaque assay. To determine rate of RNA synthesis, viral RNA was extracted from supernatants and quantified by qRT-PCR.

Virion stability

Virus stocks were diluted to 10^5 PFU/ml in culture medium and incubated at 28ºC or 37ºC. At 0, 8, 24 and 48 hours, 100 µl aliquots were taken for titration of infectivity by plaque assay

and for quantification of virus particles containing genomes by qRT-PCR. The specific infectivity was determined by dividing the infectious virus PFU values by the total number of genomes contained in the viral particles. At time zero, all virus stocks presented similar infectious titers and specific infectivities (between 0.203 and 0.217).

Fusion-blocking antibody dynamics

Antibodies CHIK102, 152, 166, 263 were a kind gift from Michael Diamond(Pal et al., 2013). To address virus fusion in the presence of blocking antibodies, ~50 PFU of each virus were incubated at 4ºC on a monolayer of Vero cells for 1 h. Cells were washed extensively with ice-cold PBS and blocking antibodies, diluted in DMEM, were added to cells for 1 h at 4ºC. To induce virus fusion, cells were incubated at 37ºC for 15 min followed by the addition of an agarose overlay. Antibody inhibition was addressed 72 hours later.

Virion purification

Viral particles were pelleted by ultracentrifugation at 25,000 x g for 2 hours at 4°C through a 20% sucrose cushion. The pellet was resuspended in sterile filtered PBS and passed three times through a 100K Ambion centrifugal filter column (Millipore) and resuspended in sterile filter PBS.

Electron Microscopy

For scanning electron microscopy HeLa and C6/36 cells were fixed in 2.5% glutaraldehyde in 0.1 M cacodylate buffer (pH 7.2), washed in 0.2 M cacodylate buffer (pH 7.2), postfixed for 1 h in 1% osmium tetroxide in 0.1 M cacodylate buffer (pH 7.2), and then rinsed with distilled water. Samples were dehydrated through a graded series of 25, 50, 75, 95 and 100% ethanol solution followed by critical point drying with CO_2. Dried specimens were sputtered with 10 nm gold palladium, with a GATAN Ion Beam Coater and were examined and photographed with a JEOL JSM 6700F field emission scanning electron microscope operating at 5 Kv. Images were acquired with the upper SE detector (SEI) .

For transmission electron microscopy, cells were fixed overnight at 4°C with 2,5% glutaraldehyde in 0.1M cacodylate buffer, pH 7.4, and postfixed in 1% osmium tetroxide in 0.1 M cacodylate buffer, pH 7.4, for 1 h. After being rinsed in 0.1M cacodylate buffer, cells were transferred to 0.2M cacodylate buffer for 30 min. Cells were washed in 30% methanol for 10 min, stained in 2% uranyl acetate-30% methanol for 1h, and washed in 30% methanol. Cells were then dehydrated in an ethanol series and embedded in Epon. Thin sections were cut with a Leica Ultramicrotome Reichert Ultracut S, stained with uranyl acetate. Purified viral particles were fixed with 2.5% gluteraldehyde in 0.1M cacodylate buffer, pH 7.4, washed twice with sterile filtered H_2O, and stained with 1% phosphotungstic acid (PTA). Images were taken with a JEOL 1200EX2 Electron Microscope at 80kV equipped with an Eloïse Keen View camera.

Immunoblotting

BHK cells were infected at an MOI=1 and incubated for 24 hours. Cells were harvested, washed with PBS, and resuspended in 2x SDS-PAGE buffer containing 5% beta-mercaptoethanol (BioRad). Proteins were separated on a 4-20% TGX-Miniprotean gel (BioRad), transferred to a nitrocellulose membrane, blocked in 5% non-fat milk in phosphate buffer saline containing 0.1% Tween-20 (PBST), and incubated with primary anti-mouse chikungunya virus E2 antibody (CHIK48 – a kind gift from Michael Diamond). Membranes were washed extensively and incubated with ECL anti-mouse IgG horseradish peroxidise (HRP) secondary antibody (GE Healthcare), and developed with SuperSignal West Pico chemiluminescent substrate (Pierce).

Normal mode analysis

Normal mode analysis of E1 and the E1/E2 dimer were conducted using the Gaussian Network Model (GNM)(Emekli et al., 2008; Haliloglu et al., 1997) and the X-ray crystal structure of chikungunya virus particles E1-E2 (PDB code: 2XFB)(Voss et al., 2010), where

E1 is in complex with E2. GNM describes the protein structure as elastic network, in which the α-carbon atoms within a cut-off radius are assumed to be connected by Hookean springs, displaying Gausssian fluctuations around their mean positions. The correlation between two nodes i and j, $\Delta\mathbf{R}_i$ and $\Delta\mathbf{R}_j$, respectively, are calculated as $<\Delta\mathbf{R}_i\Delta\mathbf{R}_j> = (3k_BT/\gamma)[\boldsymbol{\Gamma}^{-1}]_{ij} = (3k_BT/\gamma)\sum_k[\lambda_k^{-1}\mathbf{u}_k\mathbf{u}_k^T]_{ij}$

where $\boldsymbol{\Gamma}$ is an $N \times N$ Kirchhoff matrix of the inter-node contacts with the (commonly used) cutoff of 10 Å, where N is the number of amino acids in the protein. $\mathbf{u}_k$ and λ_k are the k-th eigenvectors and eigenvalues of $\boldsymbol{\Gamma}$, k_B is the Boltzmann constant, T is the absolute temperature, and γ is a uniform force constant; k_BT/γ was taken as 1 Å^2. Overall, Eq. 1 predicts the mean-square displacement of each residue when $i = j$ and the correlations between the fluctuations of residues i and j when $i \neq j$, and when $i \neq j$, it predicts the correlations between the fluctuations of residues i and j as a superimposition of N-1 eigenmodes from the slowest to fastest modes of motion. Slow modes refer to cooperative and global motions, whereas fast modes refer to the residues displaying localized fast fluctuations. The results of the analysis of E1 alone are presented in Fig. 4B and of the E1/E2 complex in Supplemented Fig. S3.

Mosquito infections and harvests

Aedes aegypti (1 lab-reared Rockefeller colony, 1 colony, F10 generation, collected in Bénoué, Cameroon in September 2007; 1 colony, F2 generations collected in Nakhon Chum, Thailand in 2011; 1 colony, F3 generations, collected in Kampong Cham, Cambodia) and *Aedes albopictus* (1 colony, F14 generation, collected in Bertoua, Cameroon in September 2007; 1 colony, F2 generations, collected in Phu Hoa, Vietnam in 2011) were used for mosquito infections. Viruses were diluted to 10^3 or 10^5 PFU/ml and mixed 1:2 with pre-washed rabbit blood. Female mosquitoes were allowed to feed on 37ºC blood meals through a chicken skin membrane for 20-60 min after which engorged females were incubated at 28ºC with 10% sucrose *ad libitum*, females that did not feed were excluded. Matched titers of

blood meals (within 0.3 $\log_{10}$ PFU/ml) were verified by titrations of blood meals immediately after feeds. After incubations, legs and wings were removed, the proboscis of each mosquito was inserted into a capillary tube containing 5 µl FBS for 45 m. Midguts, legs/wings and salivary glands were dissected in PBS under 10X magnification. Saliva samples in FBS were added to 45 µl of L-15 media and the legs/wings, bodies and salivary glands were placed in 2 ml round bottom tubes containing 300 µl DMEM and a steel ball. Samples were ground in a MM300 homogenizer (Retsch) at 30 shakes/s for 2 min. For infectivity determinations, whole bodies were ground individually, using the same homogenization methods. At least 20 mosquitoes were used per sample to ensure that enough mosquitoes fed and became positively infected for downstream analysis.

Mouse infections

Mice were kept in the Pasteur Institute animal facilities in BSL-3 isolators, with water and food supplied *ad libitum*, and handled in accordance with institutional guidelines for animal welfare and at endpoint, were humanely euthanized complying with the Animal Committee regulations of Institut Pasteur in Paris, France, in accordance with the EC 86/609/CEE directive. 8-day old C57B/6 mice were injected subcutaneously in the back with 200 PFU of virus and at selected times post-inoculation, animals were sacrificed and blood and organs were harvested. Organs were placed individually in tubes and homogenized as for mosquitoes. Survival curves were generated by injecting 8-day or 3-week old female mice with 10^6 PFU of virus and monitoring morbidity and mortality for 14 d after infection.

Transmission studies

Transmission experiments were conducted at the Institut Pasteur in Cambodia in Phnom Penh in BSL3 facilities. Briefly, mosquitoes were infected as described previously and incubated at 28°C for ten days. On day ten, individual mosquitoes were allowed to feed on individual five day old Swiss mice until engorged. 5-day old Swiss mice were immobilized on a mesh

surface suspended over a cup containing an individual mosquito at 28ºC. Mice and mosquitoes were incubated together for 1 hour or until feeding had occurred. Following feeding mice were returned to cages and individual mosquitoes were salivated and their bodies crushed and harvested. Mice were monitored for disease for five days. After five days of infection in mice, naïve mosquitoes were allowed to feed on individual infected mice until engorged. Following feeding, mice were sacrificed and blood was harvested. These mosquitoes were then incubated at 28°C for ten days, salivated and their bodies crushed and harvested. Amplicons for deep sequencing were prepared immediately after harvesting *in vivo* samples, which improved the overall yield compared to using frozen samples.

High-throughput Sanger sequencing and genetic diversity

For genetic diversity and bottleneck experiments, amplicons flanking the partial E1 gene were generated using the Titan one-step RT-PCR kit (Roche) and primers flanking genome positions 9943–10746. Amplicons were cloned into TOPO vectors (Invitrogen) and sequenced using Sanger technology in 96-well format (GATC Biotech). Mutation frequencies were determined by dividing the number of nucleotide polymorphisms in all clones (where polymorphisms at the same genetic locus on multiple clones were counted once) by the number of nucleotides sequenced. Values were then represented as number of mutations per 104 nt sequenced. Each frequency was corrected by subtracting the background mutation frequency, defined as the mutation frequency in TOPO-cloned clone plasmid DNA sequences. In vitro transcribed clone RNA subjected to the same RT-PCR and TOPO cloning demonstrated a mutation frequency that was not significantly different from cloned plasmid (data not shown), indicating that the RT-PCR was not a significant source of mutational error.

Deep sequencing of samples

Viral RNAs were isolated from samples by Trizol extraction, and the E1 gene was amplified using the Titan one-step RT-PCR kit (Roche) with the following primers: E1Forward(9943)

5′ TACGAACACGTAACAGTGATCC 3′ and E1Reverse(10726) 5′ CGCTCTTACCGGGTTTGTTG 3′ following manufacturer's instructions. PCR fragments were purified via the Nucleospin Gel and PCR Clean-up kit (Macherey-Nagel) and total DNA was quantified by Nano-drop. PCR products were then fragmented (Fragmentase), linked to Illumina multiplex adapters, clusterized and sequenced with Illumina cBot and GAIIX technology. Sequences were demultiplexed using Illumina's CASAVA software, allowing for no mismatches in the multiplex tag sequences. Quality filtering (95-98% of reads passed) and adaptor cleaning was done using fastq-clipper (http://hannonlab.cshl.edu/fastx_toolkit/index.html). The 75-nt reads were aligned to the E1 sequence as a reference, with a maximum 2 mismatches per read, using BWA(Li and Durbin, 2009). Alignments were processed using SAMTOOLS(Li et al., 2009) to obtain the nucleotide/base calling at each position. An in-house ViVAn (Virus Variance Analysis) pipeline was used to identify statistically significant variants above the background noise due to sequencing error, calculated for each nucleotide site. Briefly, for each position throughout the viral genome, base identity and their quality scores were gathered. Each variant allele's rate was initially modified according to its covering read qualities based on a maximum likelihood estimation, and tested for significance using a generalized likelihood-ratio test. Additionally, an allele confidence interval was calculated for each allele. In order to correct for multiple testing, Benjamini-Hochberg false-discovery rate of 5% was set. In all experiments, a minimum coverage of 25,000 reads was obtained and the background error at every nucleotide site was always below 0.01%.

Statistical Analyses

No samples or infected animals were excluded from analysis. Animals were randomly allocated to groups before infections were performed. No blinding was performed during experimentation and analysis. All statistical tests (described in each figure legend) were

conducted using GraphPad Prism software. P-values >0.05 were considered non-significant (ns).

Coffey, L.L., and Vignuzzi, M. (2011). Host alternation of chikungunya virus increases fitness while restricting population diversity and adaptability to novel selective pressures. J. Virol. *85*, 1025–1035.

Emekli, U., Schneidman-Duhovny, D., Wolfson, H.J., Nussinov, R., and Haliloglu, T. (2008). HingeProt: automated prediction of hinges in protein structures. Proteins *70*, 1219–1227.

Haliloglu, T., Bahar, I., and Erman, B. (1997). Gaussian dynamics of folded proteins. Physical Review Letters.

Li, H., and Durbin, R. (2009). Fast and accurate short read alignment with Burrows-Wheeler transform. Bioinformatics *25*, 1754–1760.

Li, H., Handsaker, B., Wysoker, A., Fennell, T., Ruan, J., Homer, N., Marth, G., Abecasis, G., Durbin, R., and Subgroup, 1.G.P.D.P. (2009). The Sequence Alignment/Map format and SAMtools. Bioinformatics *25*, 2078–2079.

Pal, P., Dowd, K.A., Brien, J.D., Edeling, M.A., Gorlatov, S., Johnson, S., Lee, I., Akahata, W., Nabel, G.J., Richter, M.K.S., et al. (2013). Development of a highly protective combination monoclonal antibody therapy against Chikungunya virus. PLOS Pathogens *9*, e1003312.

Voss, J.E., Vaney, M.-C., Duquerroy, S., Vonrhein, C., Girard-Blanc, C., Crublet, E., Thompson, A., Bricogne, G., and Rey, F.A. (2010). Glycoprotein organization of Chikungunya virus particles revealed by X-ray crystallography. Nature *468*, 709–712.